INVESTIGATE MATERIAL SYSTEMS FOR MIRRORS USED IN HIGH POWER CO AND CO2 LASERS

R. W. Stewart

Battelle-Pacific Northwest Laboratories

Prepared for:

Office of Naval Research
Advanced Research Projects Agency

December 1972

Battelle
Pacific Northwest Laboratories
Battelle Boulevard / Richland, Washington 99352

INVESTIGATE MATERIAL SYSTEMS FOR MIRRORS USED IN HIGH POWER CO & CO_2 LASERS

SEMI-ANNUAL TECHNICAL REPORT

DECEMBER 1972

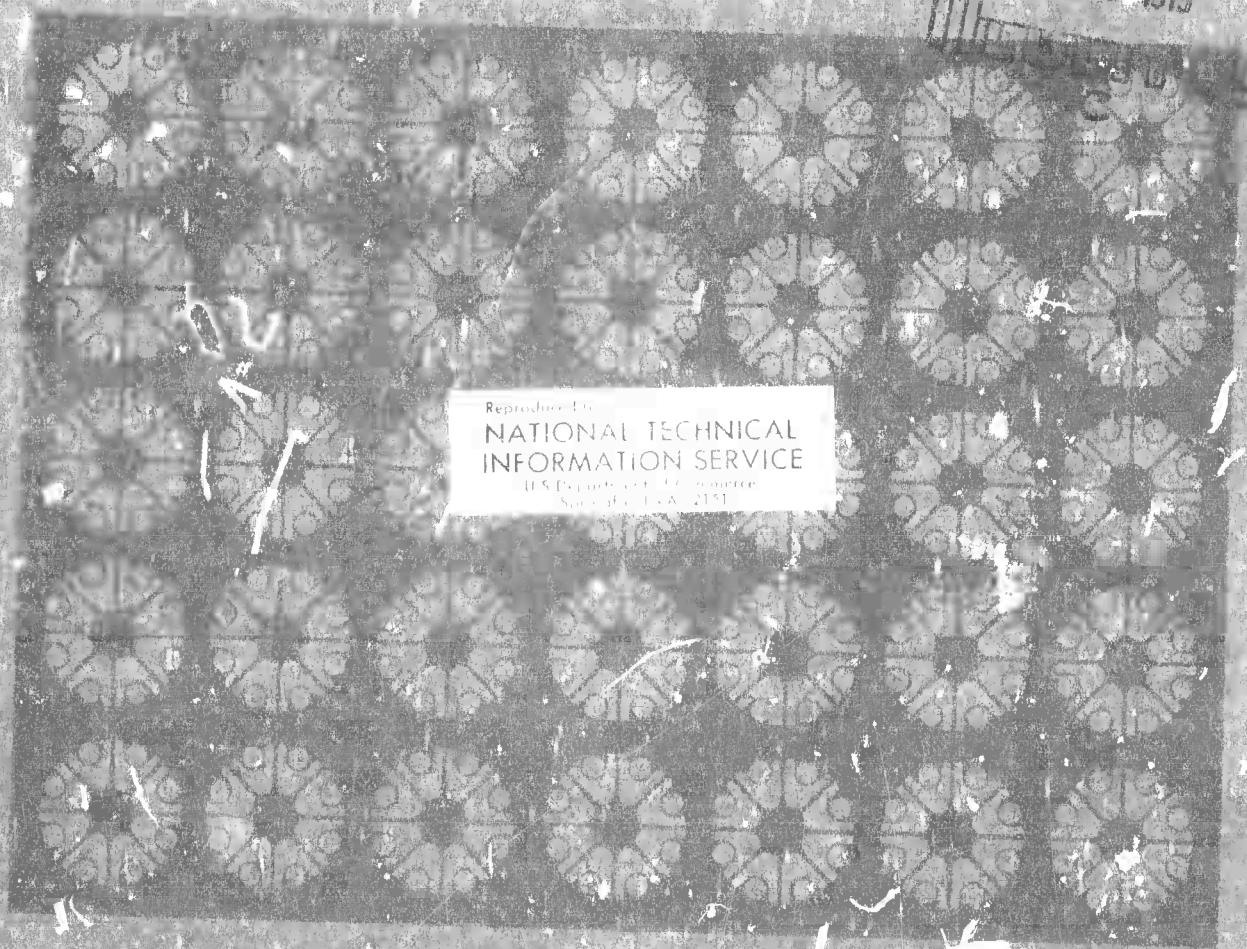

INVESTIGATE MATERIAL SYSTEMS FOR MIRRORS USED IN HIGH POWER CO AND CO_2 LASERS

Semiannual Technical Report
December 1972

Sponsored by Advanced Research Projects Agency
Contract #N00123-72-C-2215
ARPA Order No. 2175
Program Code No. 2D10

Principal Investigator
RW Stewart
509-942-2576

Effective Date
May 22, 1972

Contract Expiration Date
November 22, 1973

Amount of Contract
$450,000

BATTELLE
PACIFIC NORTHWEST LABORATORIES
RICHLAND, WASHINGTON 99352

INVESTIGATE MATERIAL SYSTEMS FOR MIRRORS USED IN HIGH POWER CO AND CO_2 LASERS

by

R. W. Stewart

ABSTRACT

Results are presented from the first phase of a three-phase program sponsored by Advanced Research Projects Agency to develop a laser mirror material system.

Copper, dispersion hardened with the addition of 0-5 vol% SiC or Al_2O_3 was deposited by high-rate sputtering to produce a stable, fine-grain (<0.4 μm) polishable material exhibiting a surface roughness of less than 15 Å rms when it was mechanically polished.

Instruments for measuring surface roughness by scattered light and mirror absorption by differential calorimetry were also designed, constructed, and successfully employed in measuring surface properties and mirror optical absorption.

CONTENTS

CONTENTS (contd)

LIST OF FIGURES

LIST OF FIGURES (contd)

LIST OF FIGURES (contd)

LIST OF TABLES

INVESTIGATE MATERIAL SYSTEMS FOR MIRRORS USED IN HIGH POWER CO AND CO_2 LASERS

by

R.W. Stewart

SEMIANNUAL TECHNICAL REPORT

INTRODUCTION

The purpose of this report is to describe progress on the first six-month phase of a program being conducted by Battelle-Northwest Laboratories in close cooperation with the Naval Weapons Center at China Lake, California to investigate materials systems for high-reflectivity infrared (IR) mirrors used in high-power lasers. Front surface, high-reflectivity laser mirrors have received increased attention in the last few years. Power densities of several kW/cm^2 are anticipated on cavity optics components, both for continuous wave (CW) and pulsed IR laser applications. It is generally conceded that mirrors for such applications require reflectivities of $\geq 99.9\%$.(1) In addition, to obtain the thermal conductivity required for heat dissipation, metal mirror components are considered essential wherever their use is feasible. The mirror structure visualized initially consists of the following components listed in their sequence of formation:

1) A metal mirror support, on which will be deposited successive layers of material by sputtering or ultrahigh vacuum evaporation. The mirror support material selected for the initial work will be OFHC (Oxygen Free High Conductivity) copper.

2) A hard, stable, fine-grained, sputter-deposited metal mirror material whose principal property will be its ability to be polished to a surface roughness ≤ 20 Å rms.

(1) C.M. Stickley, "Conference on High Power Infrared Laser Window Materials," (C.S. Sahagian and C.A. Pitha, eds.) Air Force Cambridge Research Labs Special Report No. 127, p. 405, November 1971.

3) A thin, high conductivity sputter-deposited or evaporated metal overlayer having a high-reflectivity surface.

4) A (minimum components) dielectric quarter-wavelength reflectivity enhancement coating to improve the reflectivity of the surface achieved in 3 above. The (minimum layer) limitation derives from the low conductivity of dielectric material and the realization that the expected several Watts/cm^2 absorbed power may cause spallation of the dielectric.

It is pertinent to note that although quartz has been mechanically polished to a surface roughness of <10 Å rms,[1] the best surface obtained on conventionally fabricated metals has been in the 35-50 Å rms range.[2] Sputtered deposits offer the advantages of extremely fine-grain size (<1 μ), homogeneity, and ability to dispersion harden. These features form the basis for thinking that the necessary mirror properties are obtainable through application of sputtering technology.

SUMMARY

TECHNICAL PROBLEM

The ultimate objectives are to establish the material parameters which are important to obtaining required mirror performance, and to demonstrate the validity of the developed information by the fabrication of a 1.520 in. diameter curved (r - 1.43 m) mirror having absorption of ≤0.1% of incident IR radiation (10.6 μm wavelength) and with an appropriate quarter-wavelength reflectivity enhancement coating.

The specific objectives of the first phase of the program are:

1) Investigation of the polishability of sputter-deposited material towards achieving a surface exhibiting either a surface roughness of 20 Å rms or less, or the definition of procedures necessary to attain that smoothness.

(1) R.W. Dietz and J.M. Bennett, "Bowl Feed Technique for Producing Supersmooth Optical Surfaces," J. Applied Optics, vol. 5, pp. 881-882, 1966.
(2) H.E. Bennett, Private communication.

2) Sufficient characterization of the prepared samples to allow identification of those approaches most likely to result in further improvements.

3) Development of supporting instrumentation
   a. Calorimeter for mirror absorptance measurements with 10% accuracy operational
   b. Scattered light measuring instrument operational
   c. Study of feasibility of optical heterodyne technique for roughness evaluation started.

4) Initiation of investigation of low pressure sputtering for high reflectance metal overlayer.

GENERAL METHODOLOGY

Laboratory scale application of sputtering technology to the development of a mirror structure and the characterization and evaluation of structures formed.

TECHNICAL RESULTS

The work performed to date has validated the original concept of using sputtered, dispersion-hardened stable copper as a metal mirror material capable of accepting treatment to provide surface finishes of less than 20 Å rms. The material characteristics of principal importance have been determined to be material homogeneity and small grain size ($\leq$0.4 μ). The expected correlation between hardness and polishability was not observed. The principal deposition parameters for achieving these material properties have been established with demonstrable reproducibility.

Measured absorption at λ = 10.6 μm has thus far not correlated with any characteristic other than the electrical conductivity of the mirror material. The reflectivity decreases with decreasing conductivity as expected. Maximizing reflectivity in the polishable deposit requires minimizing the dispersoid content while at the same time maintaining the

stable, fine-grain microstructure in the deposit. Variation in surface roughness below 20 Å rms does not appear to influence measured reflectivity.

Use of the bowl-feed polishing process, with a pitch lap and Barnesite dispersed in water as a polishing medium, worked well for polishing fused quartz but was not found suitable for surfacing of metals. Other liquid polishing mediums were tried with the pitch lap but they were not successful. Excellent results were obtained by changing to a cloth lap and a colloidal carbon (modified india ink) polishing medium using the same equipment. About 30% of the polished samples exhibited surfaces with less than 15 Å rms surface roughness using this polishing technique.

DEPARTMENT OF DEFENSE IMPLICATIONS

The work in the first phase has demonstrated that dispersion-hardened fine-grain metals may be mechanically polished to produce ultra-smooth surfaces. This demonstration and the anticipated results in the following phases could greatly advance laser technology.

IMPLICATIONS FOR FURTHER RESEARCH

Although adequate at the present, additional research will be required on materials properties versus performance and on polishing technique. The existing scope of the contract does not permit the research required in these areas. To prevent a future delay in program accomplishment, consideration should be given to concurrent effort in the indicated areas.

PROCEDURE AND DEVELOPMENT OF REQUIRED TECHNOLOGY FORMATION AND SAMPLING OF METAL MIRROR MATERIAL

SPUTTER DEPOSITION

The experimental materials for the mirror surface were formed on the mirror support by sputter deposition using the supported discharge, direct current mode of operation.[1,2] The target (deposition source) and substrate (mirror support) were parallel flat discs spaced about 3 cm apart in a bakeable vacuum chamber which was capable of 1×10^{-8} torr base pressure. The sputtering gas was research grade krypton from Linde.

The targets were prepared by compacting mixtures of OFHC copper powder and either silicon carbide or alumina powders in a Dyna-Pak(R) machine while simultaneously bonding the mixtures to OFHC copper backup plates. The backup plates were subsequently electron-beam welded to target supports allowing direct water cooling of the backup plates. Elevated temperatures were obtained by substituting air cooling for water cooling. The dimensions of the target material were about 9 cm in diameter and 1 cm thick.

The substrates were machined from OFHC copper and polished and cleaned as metallographic samples immediately prior to assembly in the sputtering apparatus. Each substrate (mirror support) consisted of a central disc about 4 cm (1.520 in.) in diameter for optical polishing and a concentric outer ring about 1.4 cm wide for metallurgical and analytical evaluation. The substrates were cleaned by ion bombardment (25 ma-min/cm^2 at 100 volts) before deposition to promote good deposit bonding. The deposition was continued to an approximate deposit thickness of 0.2 - 0.3 mm.

(1) S.D. Dahlgren and E.D. McClanahan, "High Rate Sputtering of Stainless Steel," 3rd Symposium on Deposition of Thin Films by Sputtering, Rochester, N.Y., p. 20, 1969.

(2) G.K. Wehner, Proceedings of Fifth International Conference on Ionization Phenomena in Gases, Munich 1961, North Holland Pub. Co., Amsterdam, Netherlands.

SPECIMEN PREPARATION

After deposition, the central disc and the outer ring were separated by machining. Two-stage replicas were made of the as-sputtered surface for correlation with the surface obtained by optical polishing. The outer rings were then sectioned for optical and electron metallography and microhardness measurements. Part of each outer ring deposit was removed from the substrate and used for determination of electrical resistivity. Microhardness and resistivity measurements were repeated after successive one-hour heat treatments at temperatures of 200, 350, 475 and 600°C. The resistivity data were converted to conductivity to permit convenient comparison with IACS.

EXPERIMENTAL VARIABLES

The experimental variables investigated were composition, sputter-deposition parameters, and substrate surface finish. Cross-correlation of these variables was not attempted because the large number of additional depositions required would have exceeded the scope of the program. The approach used was to make groups of depositions in which one variable was changed while all others were held constant. The variables are discussed in detail below:

1. Composition--Two dispersoids, silicon carbide and aluminum oxide, were employed in OFHC copper. It was originally planned to investigate six levels of each dispersoid, but sputtering-discharge stability difficulties encountered in targets containing high alumina concentrations caused these depositions to be canceled.

   Two dispersoids were selected to provide a backup in the event that stoichiometric transfer of the dispersoid constituents was not obtained in either case.

2. Sputter Deposition Parameters--In general the three main parameters of sputter deposition are the deposition rate (e.g. units of thickness/time), the substrate temperature, and the

electrical potential (e.g. bias) placed on the substrate during deposition. Since the deposition rate and substrate temperature are interrelated in their effects on material structure, only the substrate temperature was varied. Temperatures of ≈20, 150 and 250°C were selected. The lowest temperature was obtained by circulating <20°C water in direct contact with the rear face of the substrate.

Substrate bias voltages of ground (0 volts), floating (≈-20 volts), -50 volts, and -75 volts were selected to determine effect on deposit properties. The application of a bias voltage was expected to modify composition as well as structure.

3. Substrate Surface Finish--The standard surface preparation for the OFHC copper blanks used in this work was a metallographic polishing procedure concluded with a few seconds of electropolishing. Two other conditions were examined in single deposition experiments--an as-machined (<32 AA) single-point tool surface, and a sputter-deposited and metallographically polished surface.

The conditions under which each variable was examined are given in Table 1.

TABLE 1. Deposition Variables

Variable Examined	Deposition Rate μm/min	Substrate Temperature (°C)	Substrate Potential (V)	Surface Finish
Composition	1.7	20	-20	Pol
Sub Temp	1.7	--	-20	Pol
Sub Bias	1.7	20	--	Pol
Surface Finish	1.7	20	-20	--

The compositions used for investigating the last three variables were either 1 vol% SiC and/or 0.5 vol% Al_2O_3.

LAPPING AND POLISHING

LAPPING

The OFHC copper substrates (mirror supports) were polished as conventional metallographic samples. Some substrates were checked for optical figure; they exhibited approximately six fringes convexity.

The sputtered deposits (0.25 mm thick) were ground before final polishing in seven successive steps with decreasing diamond grit size. Grinding at each stage continued until marks from the previous stage were no longer visible at 40 X magnification. The grit sizes, approximate time during each step, and the lap used in each stage are shown in Table 2.

TABLE 2. Grinding and Polishing Schedule

Stage	Diamond Grit Size, Microns	Approximate Time, Min	Lap Material
1	30	10	Mylar
2	15	10	Mylar
3	15	15	Black Politex-D*
4	9	15	Black Politex-D
5	6	20	Black Politex-D
6	3	30	Black Politex-D
7	1	60	Black Politex-D

* Geoscience Instruments Corporation, Mount Vernon, New York

The Politex-D is a dense, smooth, hard polymeric polishing cloth with a slighly buffed and textured surface. Because of its small and uniform thickness (0.5 mm), it faithfully reproduces the figure of the lap.

POLISHING

Initial plans called for direct application of the bowl-feed technique as used in production of supersmooth quartz surfaces to final surfacing of metals. A bowl of ≈30.5 cm diameter, 8 cm deep, stainless steel was assembled.

Quartz samples were polished using a pitch lap and a polishing slurry of 20 g of Barnesite per liter of water. Corroborating surface roughness measurements indicated that BNW could duplicate the results obtained by the Naval Weapons Center. Application of this procedure to the mirror deposits produced a visible tarnish. Use of a light, water-soluble cutting oil (Cool-Tex) as the basis for the slurry resulted in no polishing action on the metal samples. Polishing powders of Barnesite, MgO and Cr_2O_3 suspended in Cool-Tex, and a mixture of Cool-Tex and water were tried with both pitch and cloth laps; all produced negative results.

Background in polishing techniques at BNW resulted in trying a slurry based on india ink[1,2] in conjunction with a Politex-D cloth lap. The polishing results were found to be satisfactory although additional development will probably be required to insure complete reproducibility. The polishing action is illustrated in the series of photos in Figure 1. Figure 1a shows the starting surface which resulted from a 1.5 minute polish of Sample 007 in a slurry of Cool-Tex and MgO on a Politex-D lap. The photos 1b, 1c and 1d show the surfaces which resulted after 2 min, 4 min and 9 min polishing in india ink at a 320x magnification using a 0.35 NA objective. The final surface exhibited a roughness <12 Å rms.

(1) A.M. Graeme-Thom, Laboratory Journal of Australia, vol. 1, p. 128, 1938. (Quoted by F.W. Twyman in Prism and Lens Making, 2nd. ed., p. 45, Hilger and Watts, Ltd., London, 1952.)

(2) J.D. Beardsley, "Metal Mirrors and Flats," Amateur Telescope Making, Book Two, A.G. Ingalls, ed., Scientific American, Inc., pp. 67-69, 1946.

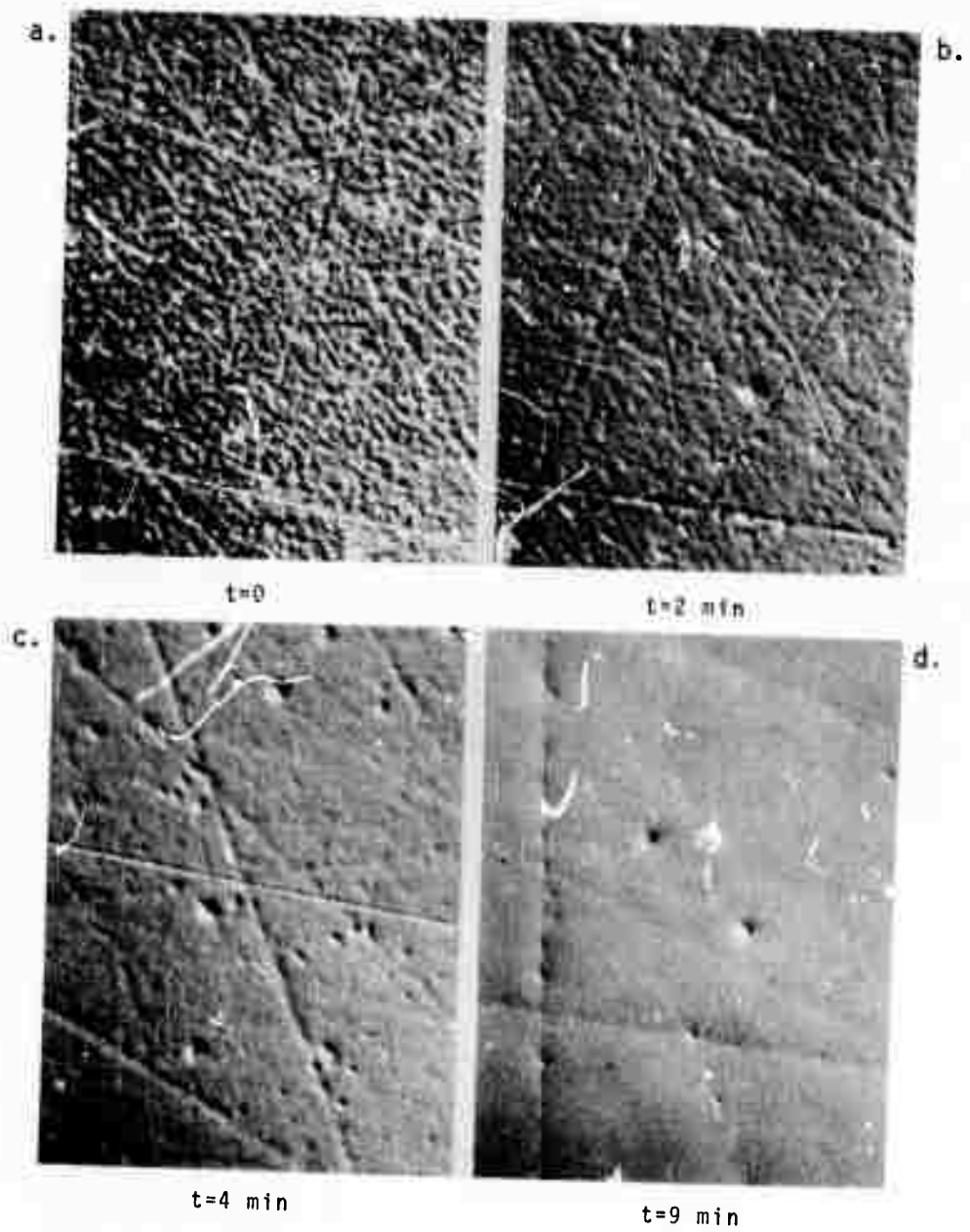

FIGURE 1. Observed Surface Changes with Polishing Time in India Ink. Sample 007

India ink* is a lyophobic sol of negatively charged carbon black particles which range in size from 7 mμ to 25 mμ. During development of the polishing technique, it was determined that agglomeration of carbon particles caused a high scratch density. It was found, however, that the particles could be maintained in suspension by the addition of a weak ammonium-hydroxide solution which increased the pH of the slurry. The slurry found to produce the most satisfactory results consists of equal parts of india ink and distilled water with 6 drops of NH_4OH per ounce of solution. The slurry is poured into the bowl and, while being stirred by the action of the paddle, one drop of a weak nonionic detergent-water solution is added as a protector. The detergent solution consisted of one drop of Ivory liquid in 10 ml distilled water. The pH of the solution must be periodically checked and maintained between 8.8 and 9.3.

Surface finish was found to be sensitive to the pressure applied to the samples during polishing. Initially, an effort was made to minimize the pressure to avoid excessive heating of the metal. Inadequate weight, however, produced very poor surfaces. The optimum pressure determined for samples polished during this phase was about 91 g/cm^2. The polishing time was also found to be an important parameter. A polishing time of 9 minutes most consistently produced good results on sufficiently homogeneous, fine-grained materials. An extended polishing period tends to produce small pits and texturing on the surface. This tendency is illustrated by comparing Figure 2, which shows Sample 007 after 11 minutes polishing time, to Figure 1d.

In the latter stages of this phase, the supplier of Politex-D cloth changed their production procedures. They now produce a grey cloth and market it as "Politex-D." This cloth is somewhat harder than the black cloth used earlier, and it is not as suitable for polishing with ink. This was demonstrated by the apparent decrease in quality of optical surfaces produced in the last two months of this phase.

* Higgins #4417 Drawing Ink

FIGURE 2. Surface of Sample 007 After 11 min Polishing Time in India Ink

Efforts during this phase were directed primarily towards production of surfaces with rms roughness of less than 20 Å rms in order to demonstrate the usefulness of sputtered materials. Consequently, little work beyond the establishment of a minimally suitable polishing technique was performed. Further work to refine and define the process is required.

SURFACE EVALUATION

SCATTERED LIGHT MEASUREMENT

An instrument for the relative measurement of surface roughness based on light scattering from the surface has been assembled and used. A detailed description of the instrument and typical data are given in Appendix A. Briefly, the intensity of He-Ne laser light scattered at an angle θ by the test sample is compared to that scattered at θ by a standard quartz sample provided by the Michelson Laboratory, China Lake, California. The standard exhibits a surface roughness of 10.83 Å rms. Forward scattering measurements are made for $20° < \theta < 75°$ from the surface normal at 5° intervals. The angle of incidence is 5°.

A number for surface roughness is obtained by means of a simple analysis based on a theory presented by Bennett and Porteus.(1) Let $w_s(\theta_i)$ and $w_n(\theta_i)$ represent the ratio of light scattered into angle θ_i to specularly reflected light, by the standard s and sample n respectively, and let $\Omega_n(\theta_i)$ be the ratio

$$\Omega_n(\theta_i) = \frac{w_n(\theta_i)}{w_s(\theta_i)} \quad . \tag{1}$$

(1) H.E. Bennett and J.O. Porteus, "Relation Between Surface Roughness and Specular Reflectance at Normal Incidence," J. Opt. Soc. Am., vol. 51, pp. 123-129, 1961.

It can be shown that, to first order, this ratio is equal to the square of the ratio of surface roughness δ_n and δ_s:

$$\Omega_n(\theta_i) = \left(\frac{\delta_n}{\delta_s}\right)^2 . \tag{2}$$

The average value of $\Omega_n(\theta_i)$ is then found to be

$$\overline{\Omega}_n = \sum_{i=1}^{m} \Omega_n(\theta_i)/m , \tag{3}$$

where m is the total number of angles at which data were taken. The sample roughness is then estimated by

$$\delta_n \sim \sqrt{\overline{\Omega}_n} \cdot \delta_s . \tag{4}$$

Corroborating measurements at Michelson Laboratory have verified this technique.

Additional information can be obtained from the angular distribution of scattered light. Plots of $\Omega_n(\theta)$ versus θ for samples with roughness less than 35 Å exhibit at least two maxima, usually near $\theta = 35°$ and $\theta = 60°$. These scattering maxima can be related to periodicities in the surface by the grating formula

$$\Lambda = \frac{\lambda}{\sin\theta_2 - \sin\theta_1} , \tag{5}$$

where Λ, θ_2, θ_1, and λ represent the spatial wavelength in the surface, the scattering angle at a maximum, the angle of incidence, and the wavelength of the incident light, respectively. In the BNW instrument $\theta_1 = 5°$ and $\lambda = 6328$ Å. BNW data, therefore, indicate dominant periodicities near $\Lambda = 1.3$ μm and $\Lambda = 0.8$ μm. At this time it is not known if the periodicity is due to material characteristics or if it is a result of the polishing procedure.

SURFACE PROFILE BY OPTICAL HETERODYNE

As part of the investigations of surface evaluation techniques, a theoretical analysis with preliminary design and estimated cost for an optical heterodyne surface profile instrument was made. This study is included as Appendix B. This approach appears to be feasible and an instrument of this type should yield surface profile information on the atomic scale. Further, an independent presentation[1] has since been given in which the operation of such a system has been demonstrated.

NOMARSKI DIFFERENTIAL INTERFERENCE CONTRAST MICROSCOPY

Differential Interference Contrast (DIC) microscopy had been identified in the original work plan as a method for evaluating polished surfaces. Although the method had been used in the past for examining polished surfaces, it had never been employed to examine metallic surfaces of <20 Å rms roughness. Very early in the work, while establishing polishing procedures for quartz, the DIC method was found to be very powerful in revealing textures on polished surfaces having a roughness of <20 Å rms. DIC microscopy was used continually during the development of the BNW polishing process. It became the primary evaluation tool prior to completion of the scattering instrument and calorimeter.

Nomarski DIC micrographs were made of all surfaces prepared during the first phase. A standardized magnification of 320X was used for all specimens. A Zeiss ultraphot microscope was used with a 16X Epiplan objective of 0.35 N.A., because this objective provided the best contrast. Objectives were used at nearly full aperture to obtain highest resolution; the field stop aperture was reduced to the minimum permitted by the plate scale to maximize contrast.

(1) L.J. Laub, "Acousto Optical Profilometer Suitable for Rapid Display of Surface Topography," Presented at Electro Optics Conference, New York, N.Y., September 1972.

DIFFERENTIAL CALORIMETER

A twin-type calorimeter was designed, built and calibrated to make accurate measurements of the absorbed power when the test mirrors were illuminated with 10.6 μm electromagnetic radiation. Details of the design and calibration are given in Appendix C.

After the mirror is mounted in the test cell of the calorimeter and the system has reached thermal equilibrium, a Coherent Radiation Labs (CRL) Model 42 CO_2 laser is turned on and allowed to stabilize and the output beam is intercepted by an electrically controlled shutter. The shutter is then opened and the laser beam illuminates the central portion of the test mirror. Reflected energy is measured by a CRL Model 201 power meter positioned at 3°47' from the mirror normal. By adjusting the exposure time and laser output power, each measurement is made to correspond to approximately 3 joules of absorbed energy in the sample mirror.

Data are reduced by planimeter integration of the chart records of both the time versus temperature history of the calorimeter and of the reflected power versus time curve observed on the power meter. The calorimeter calibration constant was determined to be 0.4799 ± 0.01 joules/in.^{2} of the calorimeter chart. The calibration of the power meter chart is checked on each exposure. For $E_a(E_r)$ as the absorbed (reflected) energy, the absorption α is given by

$$\alpha = \frac{E_a}{E_a + E_r} \quad . \tag{6}$$

The reflectivity is then given by $R = 1 - \alpha$. Good agreement between BNW results and total reflectivity measurements at the Michelson Laboratory were obtained.

METALLURGICAL EVALUATION

The microstructure, hardness and electrical conductivity of the sputtered deposits were sensitive to composition and substrate temperature; they were less sensitive to substrate bias. The variation of microhardness and electrical conductivity with composition (expressed as vol% dispersoid) is shown in Figure 3. Two hardness values are shown for the 0 vol% dispersion deposits, i.e., 70 and 230 DPH. The lower value was obtained after the deposit had recrystallized. Recrystallization of sputtered copper at room temperature has previously been observed[1] but only in deposits formed with ≥-50 volts bias on the substrate. The higher hardness value was obtained on a second 0 vol% deposit within a few hours after completion of the deposition and before recrystallization. The 230 DPH hardness in this pure copper deposit is attributed to its unrecrystallized microstructure, i.e., fine-grain size, high-defect density, etc. Considering this value, the major effect of adding dispersoid then, is to prevent room temperature recrystallization in the deposit. The increase in the hardness associated with the increasing dispersoid content was only about 90 DPH, i.e., 230 to 320 DPH.

It would appear from the data in Figure 3 that the smallest addition (0.25 vol%) of either dispersoid was sufficient to prevent recrystallization; this was true for the period of a week between the deposition and the hardness measurements. However, later re-examination of the 0.25 and 0.50 vol% deposits indicated that partial recrystallization had occurred. Under the present deposition conditions, between 0.50 and 1.0 vol% dispersoid was required for long-term stability of the as-deposited grain structure.

It was not possible to prepare a sample of pure sputtered copper for electrical conductivity measurement before the material recrystallized.

(1) J.W. Patten, et al., "Room Temperature Recrystallization in Thick Bias Sputtered Copper Deposits," J. Appl. Phys., vol. 42, pp. 4371-4377, 1971.

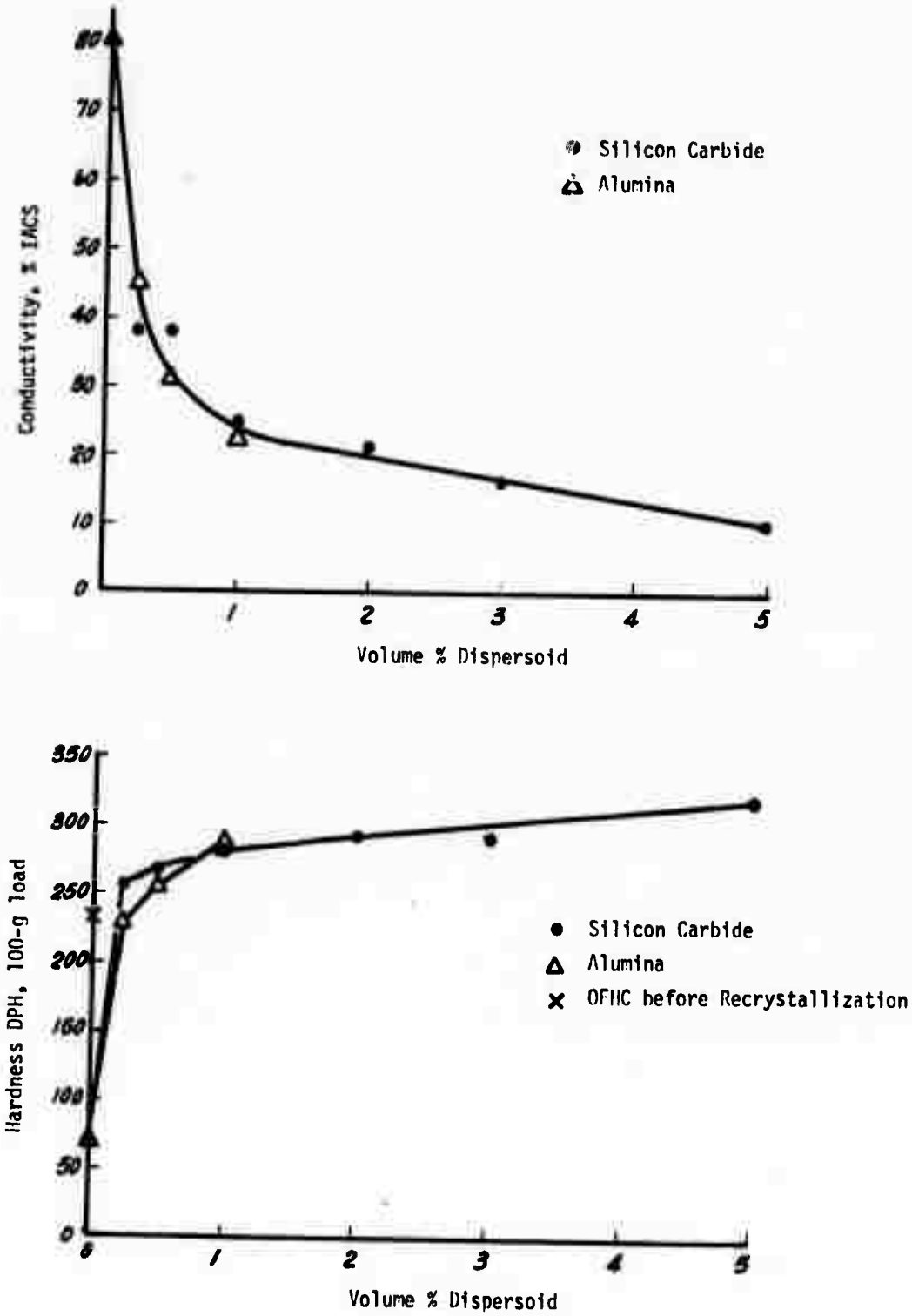

FIGURE 3. Electrical Conductivity and Microhardness of Sputtered Copper-Silicon Carbide and Copper-Alumina Versus Volume Percent Dispersoid--All Deposits Were Made on Cold (≃20°C), Electrically Floating Substrates at Approximately Equal Rates. Data Refer to the As-Deposited Condition; See Text for Discussion of 0 vol% Data.

It is believed, however, that the same type of separation of pure dispersion effects and microstructure effects (prevention of recrystallization) would apply.

The effects of changing substrate temperature and bias voltage on conductivity and microhardness are shown in Figures 4 and 5. These variables were investigated at the (constant) composition levels of 1 vol% SiC and 0.5 vol% Al_2O_3. For the temperature experiments, the substrate was electrically floating (≃-20 V bias). Increasing the temperature resulted, as expected, in a conductivity increase and hardness decrease via an in situ annealing process.

The effects of variation in substrate potential were less pronounced. The application of negative biases of -50 and -75 volts increased the conductivity 5 to 10%; there was no significant difference between samples deposited at ground (0 V) and floating (-20 V) potentials. These results can be explained by the effect of a negative bias applied during deposition in reducing the dispersoid content in the deposit. This has been observed by others in impurities and alloying elements.[1,2,3] The corresponding changes in microhardness were small and inconsistent.

Metallographic examination indicated that the grain size of the deposits containing SiC varied inversely with composition and directly with substrate temperature (Figure 6). Such variations were not observed with changing bias voltage. Variation in grain size in the deposits containing Al_2O_3 could not be related to any of the deposition parameters. The lack of correlation may have been due in part to an involuntary variation in deposition rate. Lower deposition rates had to be used in order to reduce the arc discharge instabilities. The arcing frequencies were particularly high using high percent Al_2O_3 targets.

(1) J.M. Seeman, "Bias Sputtering; Its Techniques and Applications," Vacuum, vol. 17, p. 129, 1967.
(2) L.I. Maissel, Physics of Thin Films Vol. III, p. 228, Academic, New York, N.Y., 1966.
(3) S.D. Dahlgren, A.G. Graykeel, "Reduced Nickel Concentration in a Stainless Steel Deposit from Bias Sputtering," J. Appl. Phys., vol. 41, p. 3182, 1970.

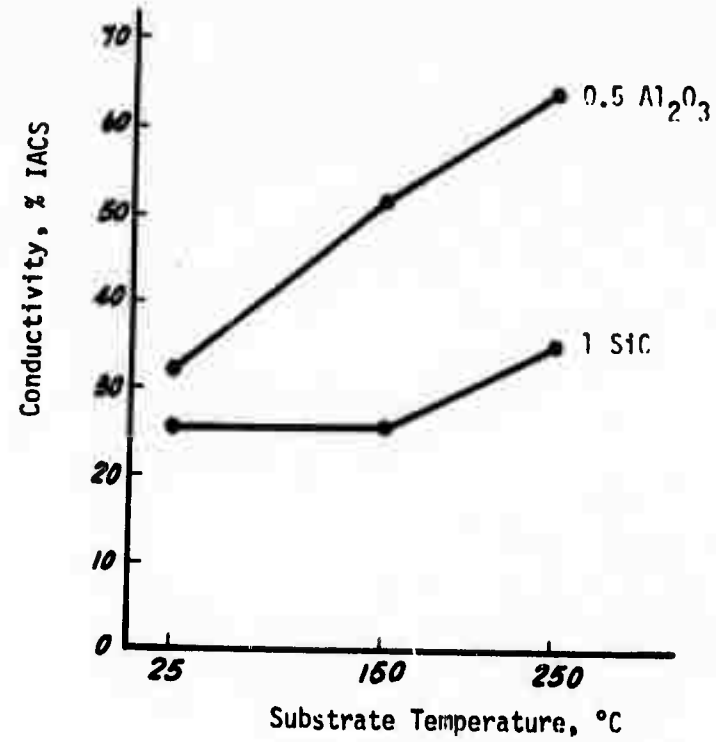

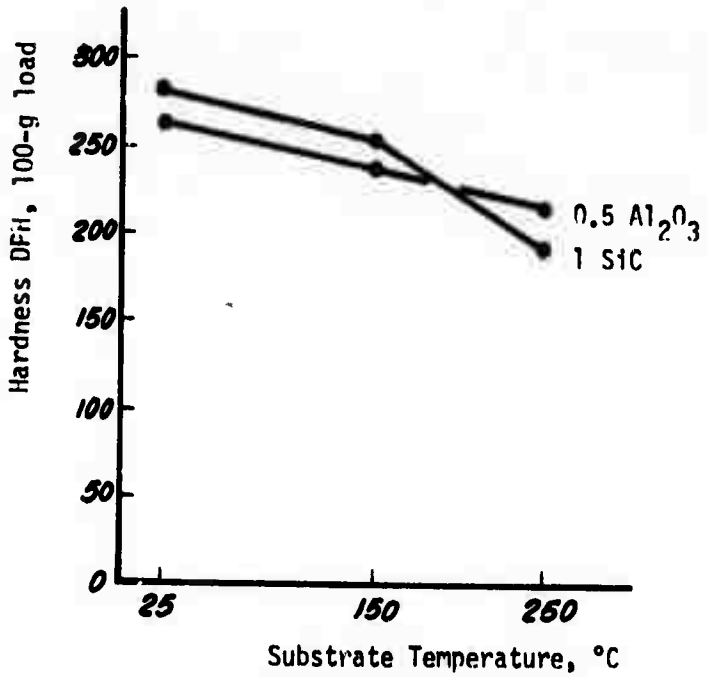

FIGURE 4. Electrical Conductivity and Microhardness of Copper 1 vol% Silicon Carbide and Copper 0.5 vol% Alumina Versus Substrate Temperature--Substrates Were Electrically Floating.

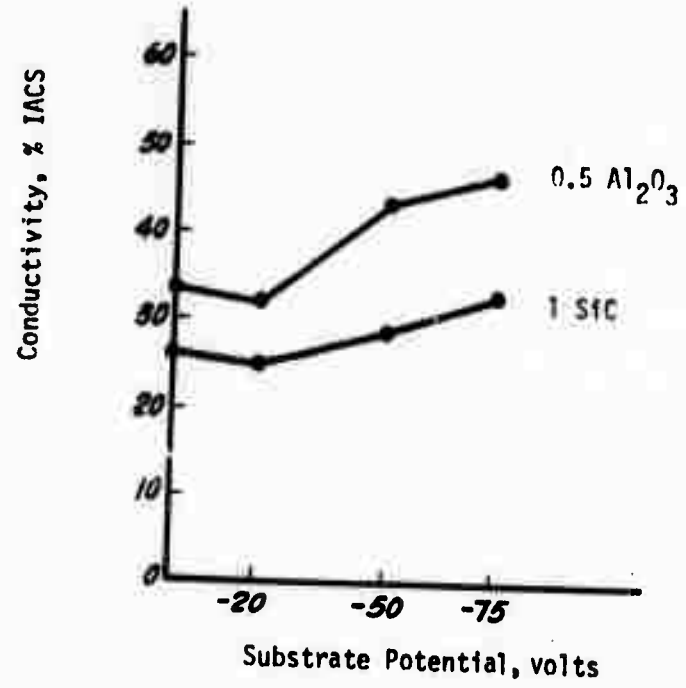

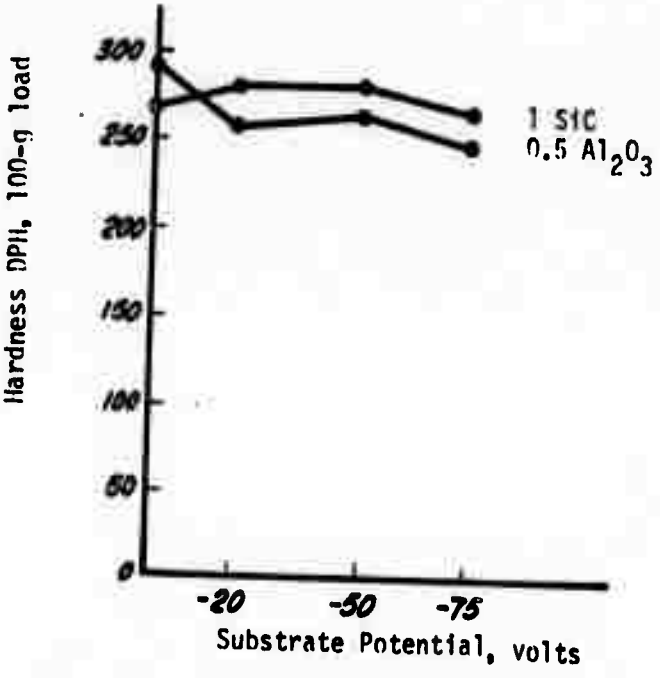

FIGURE 5. Electrical Conductivity and Microhardness of Copper 1 vol% Silicon Carbide and Copper 0.5 vol% Alumina Versus Sub-Strate Potential--Substrates Were Maintained at ≃20°C.

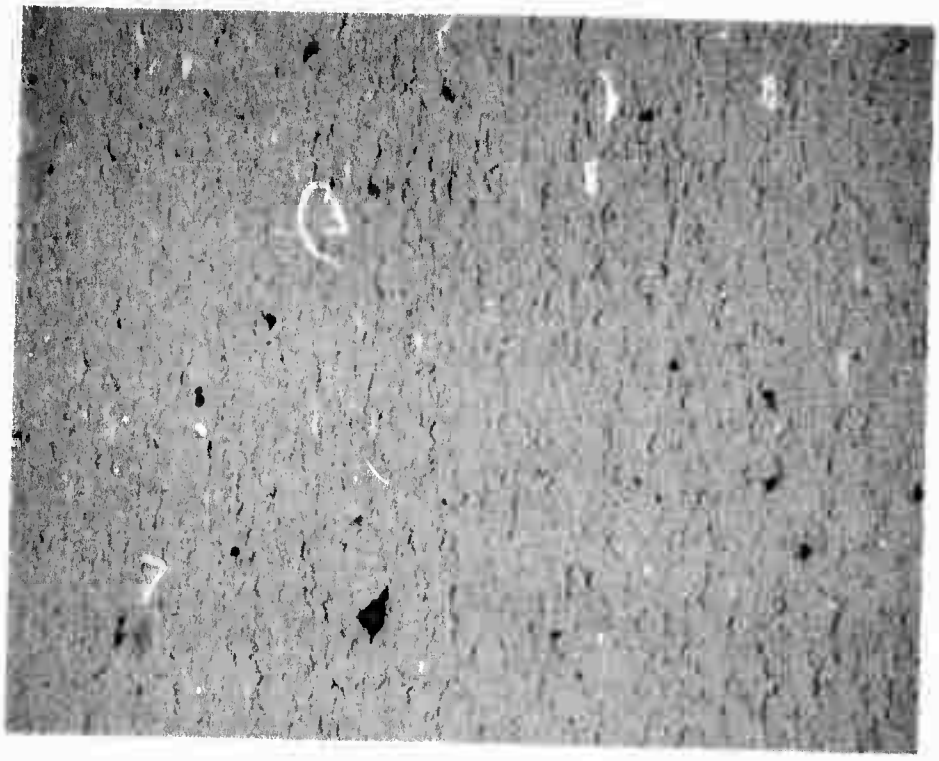

⊢ 2.5 μm ⊣

FIGURE 6. 1 vol% SiC Deposited on a Cold, Electrically Floating Substrate

Typical microstructures of the deposits containing SiC are shown in Figures 6 to 8. All deposits had the columnar grain structure typically observed in metals sputter-deposited at low to moderate substrate temperatures. The variation in grain size with composition and substrate temperature can be seen by comparing Figures 6, 7 and 8; the numerical data are plotted in Figure 9.

It was not possible to positively identify the dispersoid particles on the micrographs. This could be the consequence of one or more factors.

1) The typical diameter of a dispersoid particle could be less than the resolution of the two-stage plastic replica, 100 to 200 Å.

2) The dispersoid could be distributed largely in the grain boundaries, and thus, not be visible due to the etching behavior of the boundaries.

⟵ 2.5 μm ⟶

FIGURE 7. 0.25 vol% SiC Deposited on a Cold, Electrically Floating Substrate--The Smaller Amount of Dispersoid Resulted in a Coarser Grain Size (Compare Figure 9)

3) The dispersoid constituents could be retained in solution in the copper matrix. Although this is a reasonable possibility in view of the high deposition rates, no changes in the copper lattice parameter were observed. At least in the case of Cu-Al, such changes would be expected as a consequence of solution formation. In Cu-Si, such changes are of the order of 10^{-3} Å at.%, therefore, they are not useful to monitor solution behavior.

The as-deposited hardness values and electrical conductivities were both much lower than anticipated on the basis of previous experience with similar systems. The principal difference between the present and the earlier work was the much higher deposition rates in the present case. Since high deposition rates promote the formation of solid solutions, a

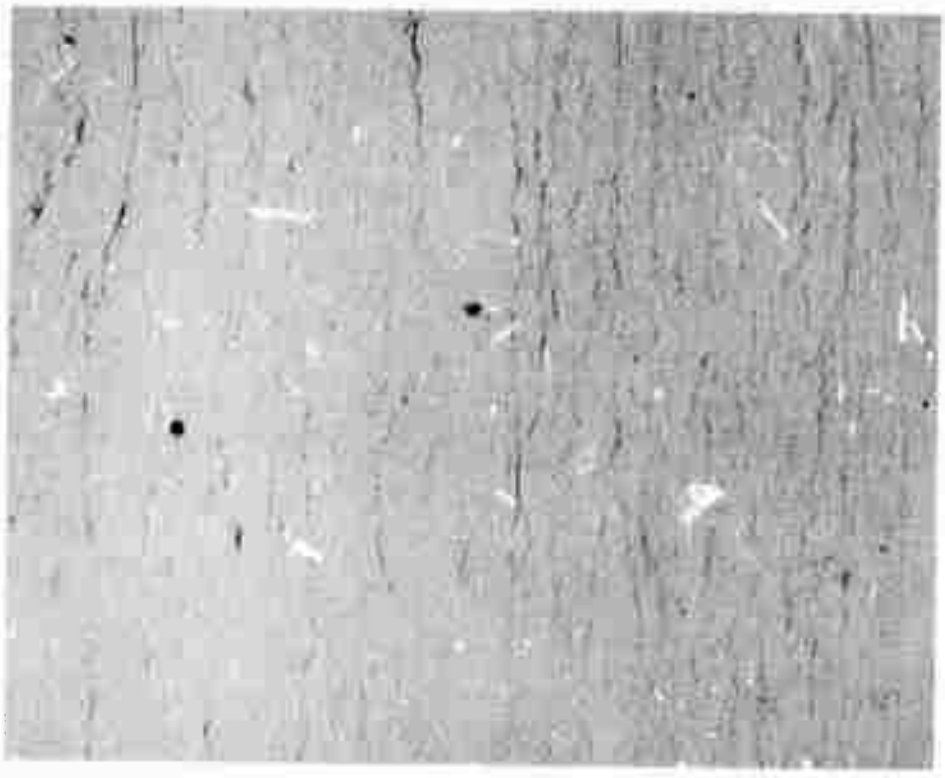

⟵ 2.5 μm ⟶

FIGURE 8. 1 vol% SiC Deposited on a 250°C, Electrically Floating Substrate--The Larger Grain Size Resulted from the High Substrate Temperature (Compare Figure 9).

heat treatment study was performed. If the heat-treated samples exhibited increases in hardness and conductivity, the low values for these properties in the as-deposited condition would be accounted for. Also, the properties of the mirror material could then be optimized by duplicating the heat treatment.

The results obtained are shown in Figure 10 (SiC containing samples) and Figure 11 (Al_2O_3 containing samples). The only samples which exhibited significant age hardening were the 3 and 5 vol% SiC deposits. These did not not show a corresponding change in conductivity. No other samples showed property changes of the magnitude expected for precipitation from solid solution.

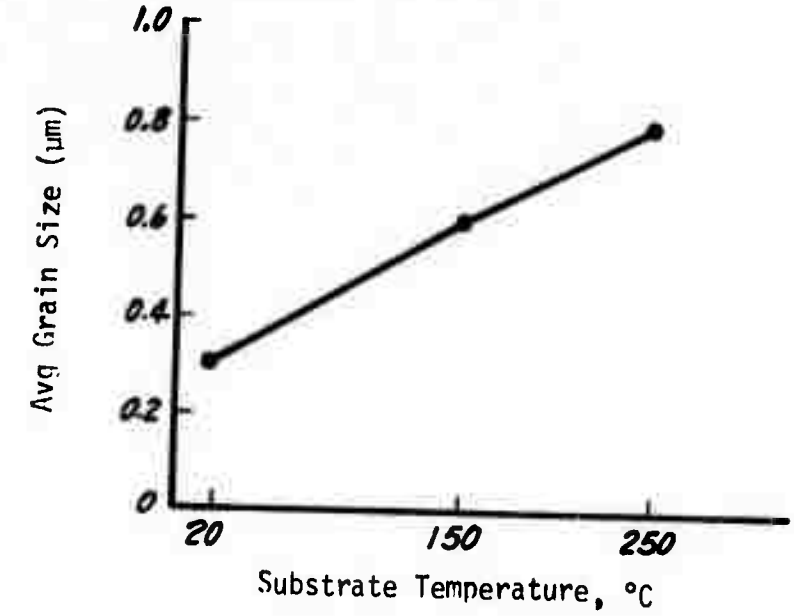

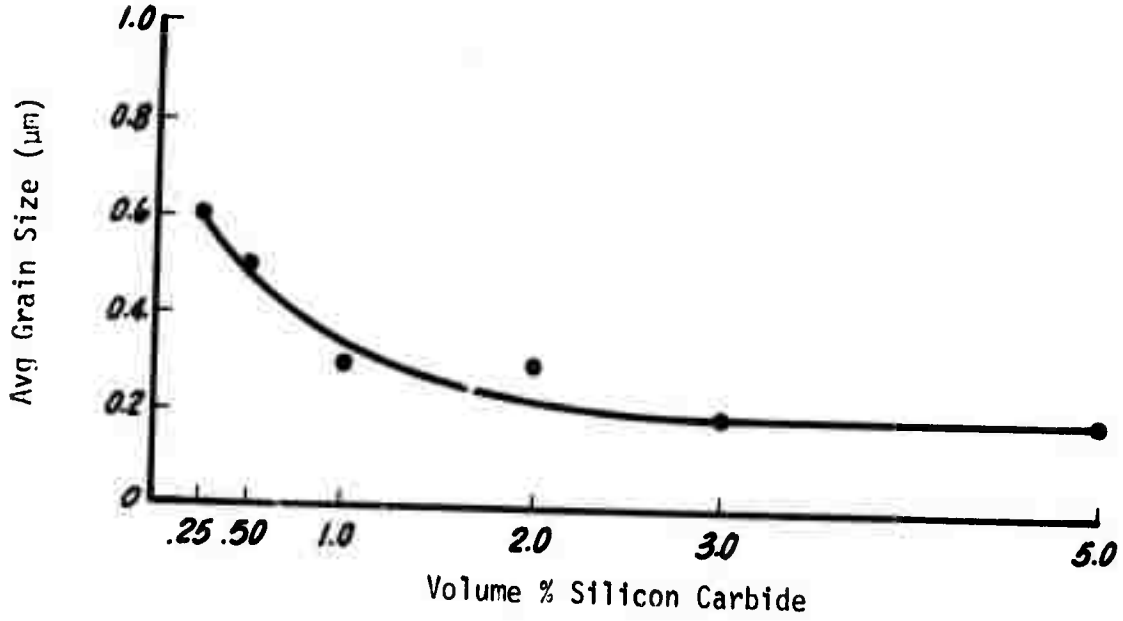

FIGURE 9. Grain Size of Copper-Silicon Carbide Deposits Versus Substrate Temperature and Volume Percent Dispersoid--The Grain Size Plotted Is the Average Diameter of the Columnar Grains Observed in Electron Replica Micrographs Such as Figures 7-9.

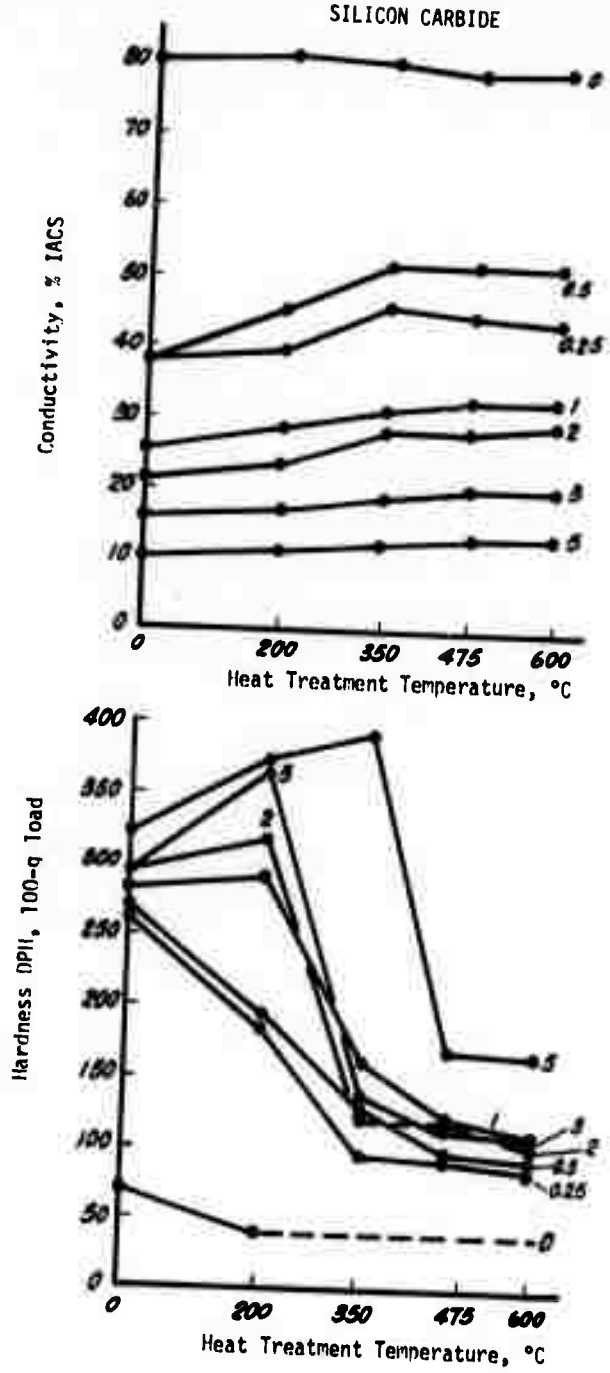

FIGURE 10. Electrical Conductivity and Microhardness of Copper-Silicon Carbide Deposits Versus Temperature of Heat Treatment (one hour at temperature) -- Numbers on the Figure Indicate Vol% Silicon Carbide. Only the 3 and 5 Vol% Deposits Exhibit Significant Age Hardening, and No Deposits Exhibit the Expected Increase in Conductivity Due to Precipitation from Solution.

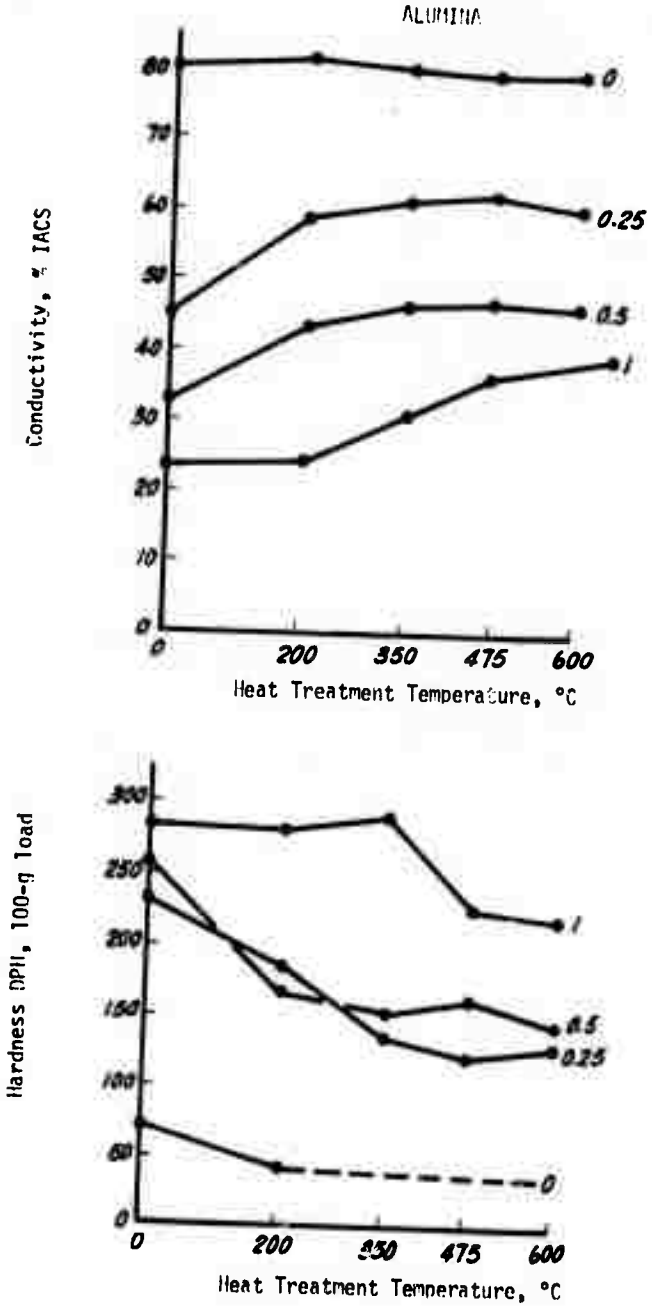

FIGURE 11. Electrical Conductivity and Microhardness of Copper-Alumina Deposits Versus Temperature of Heat Treatment (one hour at temperature) ---Numbers on the Figure Indicate Vol% Alumina. No Age Hardening Behavior is Observed.

Several samples of the deposits containing SiC were heat treated at 900°C to establish the presence of SiC in compound form by X-ray diffraction. In the 3 and 5 vol% SiC deposits, SiC reflections were observed. Samples receiving heat treatment up to 600°C showed no reflections other than those indexable as copper. Apparently the lower heat-treatment temperatures produced a small SiC particle size which resulted in the broadening of the x-ray reflections, and thus, made identification difficult.

The presence of a dispersoid is clearly indicated by the absence of significant grain growth during heat treatment at 900°C. The effect of an insoluble dispersoid in retarding grain growth can be seen by comparing the 1 vol% SiC deposit illustrated in Figure 12, with the nominnally pure copper deposit illustrated in Figure 13. Both samples were exposed to 900°C for one hour.

The nominally pure copper sample was heat treated, not only for a grain growth comparison, but also in an attempt to increase the conductivity above the somewhat disappointing 80% IACS level. No increase in conductivity was observed, apparently, because the conductivity was limited by precipitated krypton gas. What are believed to be gas bubbles are visible in the high magnification micrograph in Figure 13; it may be noted that the grain boundaries are preferred locations for bubbles. This concentration of bubbles at grain boundaries can be expected to magnify the effect of the gas on the conductivity, since it results in reduced contact area between grains.

CORRELATION OF EXPERIMENTAL VARIABLES AND METALLURGICAL CHARACTERISTICS WITH OPTICAL PERFORMANCE

To facilitate the correlation of experimental variables and metallurgical characteristics with optical performance, all pertinent data are assembled in Table 3. In general, the surface roughness, as measured by light scattering, could not be correlated with any of the deposition parameters on a one-to-one basis. As discussed below, this was influenced by several factors.

⊢ 250 μm ⊣

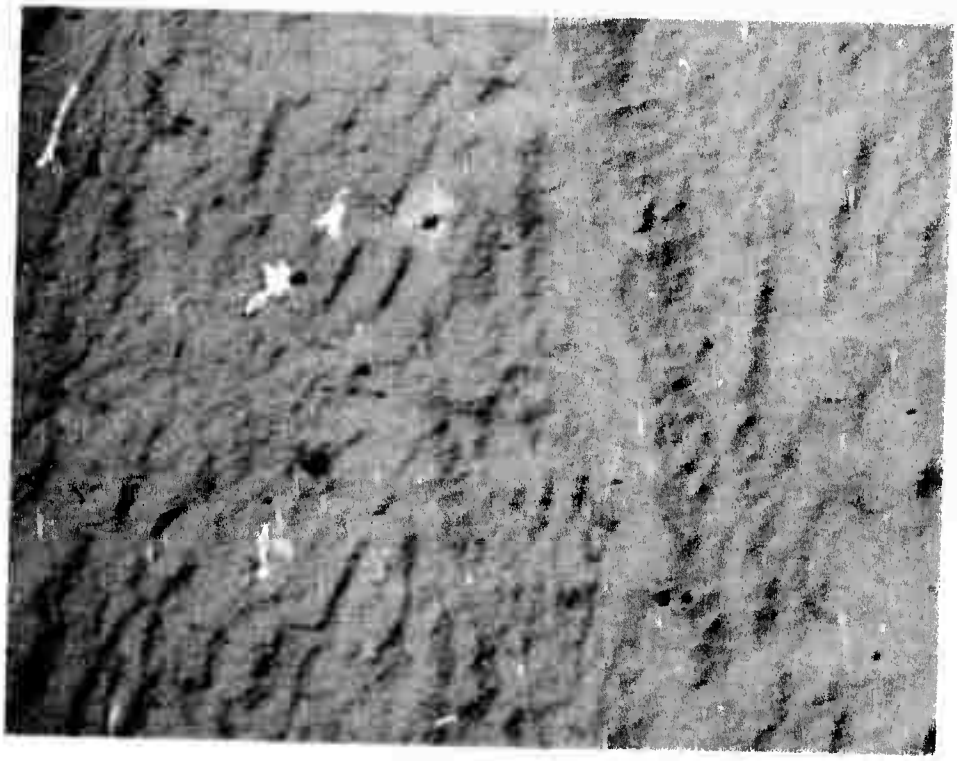

⊢ 2.5 μm ⊣

FIGURE 12. 1 vol% SiC Deposited After Annealing One Hour at 900°C -- The Effect of the Dispersion in Restricting Grain Growth Can Be Seen by Comparison With Figure 13.

⟵ 250 μm ⟶

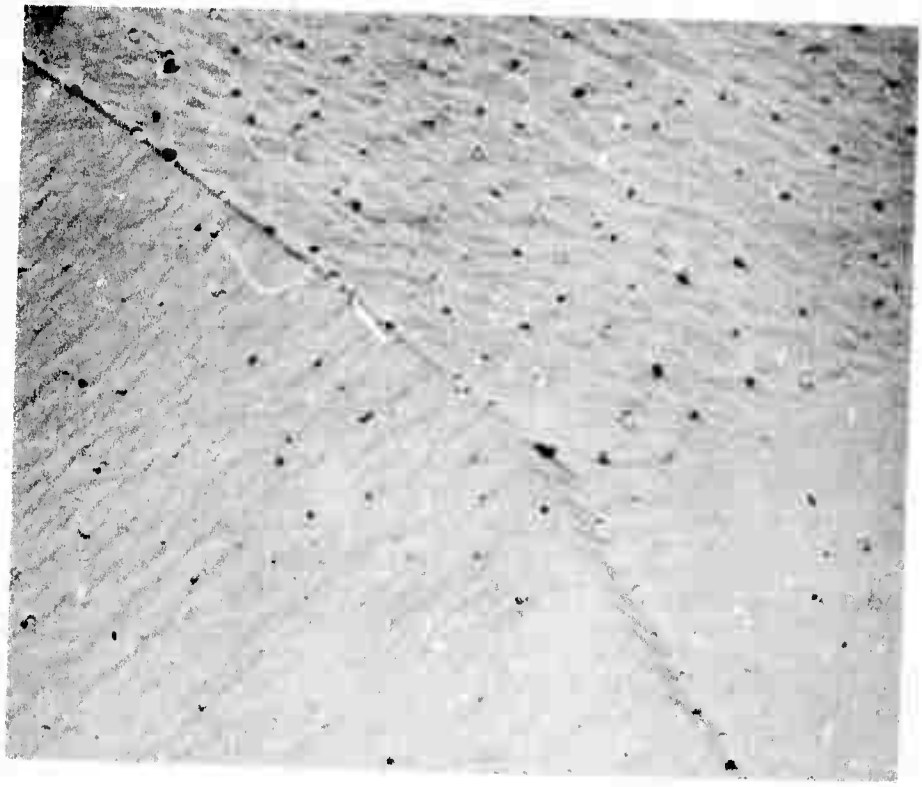

⟵ 2.5 μm ⟶

FIGURE 13. OFHC Copper Deposit After Annealing One Hour at 900°C -- The Round Defects Visible in the High Magnification Micrograph Are Believed to Be Krypton Bubbles.

TABLE 3. Composition, Experimental Variable, Property and Performance Data

Composition vol% SiC	Substrate Temp. °C	Substrate Bias V	Hardness DPH	Grain Size μm	Electrical Conductivity % IACS	Surface Roughness Å rms	Absorption %
0.25	20	-20	256	0.6	38	19	--
0.50	20	-20	267	0.5	38	> 34	--
1.00	20	-20	279	0.3	25	> 20	1.65
2.00	20	-20	293	0.3	21	> 17	--
3.00	20	-20	293	0.2	16	12	2.53
5.00	20	-20	324	0.2	10	13	--
1.00	20	-20	279	0.3	25	> 20	1.65
1.00	150	-20	251	0.6	25	--	--
1.00	250	-20	193	0.8	35	> 20	1.31
1.00	20	0	268	0.3	27	11.7	1.67
1.00	20	-20	279	0.3	25	> 20	1.65
1.00	20	-50	278	0.2	29	10	1.71
1.00	20	-75	269	0.3	33	14	1.51
Composition vol% Al_2O_3							
0.25	20	-20	228	0.3	45	12	1.15
0.50	20	-20	261	0.4	32	21	1.15
1.00	20	-20	282	0.4	23	17	1.28
0.50	20	-20	261	0.4	32	21	1.15
0.50	150	-20	0	0.5	51	--	--
0.50	250	-20	0	0.5	64	--	--
0.50	20	0	296	0.5	34	24	--
0.50	20	-20	261	0.4	32	21	1.15
0.50	20	-50	263	0.3	43	--	--
0.50	20	-75	250	0.3	46	--	--
0.00	20	-20	72	25-40	74	18	0.90
0.00	20	-20	65	30-40	80	> 20	0.88

1) Composition--Surfaces with roughness of less than 15 Å rms were produced on both alumina and silicon carbide-bearing deposits. Although the roughness values obtained were not related to the volume percentage of dispersoid, the surfaces produced on the 0.25 and 0.50 vol% SiC deposits were rougher than those on deposits with higher contents. This may be related to partial recrystallization in the deposits. In the alumina-bearing samples, on the other hand, the smoothest surface was obtained with only 0.25 vol% Al_2O_3. It should be remembered that all compositions given are nominal, since the analytical work is still in progress.

2) Substrate Temperature--Any variation of surface roughness with substrate temperature was obscured by the loss of all but one elevated temperature sample; one sample was lost through delamination of the deposit and two others were lost by the accidental deposit removal by excessive grinding. The remaining sample had a high roughness value. The observed relationship between smooth surfaces and fine-grain structure together with the known variation of grain size with substrate temperature, permit the conclusion that low substrate temperatures are desirable.

3) Substrate Bias--No consistent dependence of surface roughness on substrate bias was observed. In the silicon carbide-bearing samples, roughness of less than 15 Å rms was obtained at three out of four (0, -50, -75 Volts) of the bias levels selected. The floating substrate (-20 V) sample had a higher roughness value. The alumina-bearing samples with applied potentials (-50, -75 Volts) were lost by accidental deposit removal by excessive grinding.

4) Substrate Surface Roughness--On the basis of the three deliberate experiments performed, it was found that the smoothest final surface was obtained by depositing the hardened material on the smoothest possible substrate. This conclusion was corroborated by other BNW experience.

Attempts were made to relate the optical properties of the polished deposits to their metallurgical characteristics: microhardness, grain size, and electrical conductivity. No relationships between microhardness and surface roughness were observed; however, all samples with <15 Å rms roughness had a hardness of 225 DPH or greater. A linear relation was not obtained between grain size and surface roughness; however, all samples with <15 Å rms roughness had grain diameters in the range of 0.2 - 0.4 μm. Only two samples which had such a fine-grain size failed to develop a surface with <15 Å rms roughness. Values of grain size and microhardness can be specified which will permit the attainment of very smooth surfaces, but variation in either polishing procedure or an unmeasured material property may prevent such a sample from developing a good surface.

A linear correlation was established between the electrical resistivity and the percent absorption at 10.6 μm, (Figure 14). The measured absorption values were in fair agreement with values calculated from the resistivity according to the modified Drude theory,[1] but they were typically 5 - 10% lower. The difference may be due to a lower resistivity in the surface layer of the deposit due to relaxation of stress. A decrease of 10% in the resistivity could reasonably occur in the period (1-4 days) between the preparation of the final surface and the absorption measurement. Alternatively the bulk resistivity might have decreased a few percent in the 8-10 weeks between the resistivity measurement and the absorption measurement. However, such a decrease would have been greater in the lower dispersoid content deposits which had relatively low resistivities. Thus, the discrepancy between measured absorption and that calculated from the resistivity would have been greater at the lower resistivities; this was not observed.

(1) H.E. Bennett and J.M. Bennett, "Validity of the Drude Theory for Silver, Gold and Aluminum in the Infrared," Optical Properties and Electronic Structure of Metals and Alloys, North Holland, Amsterdam, p. 175, 1966.

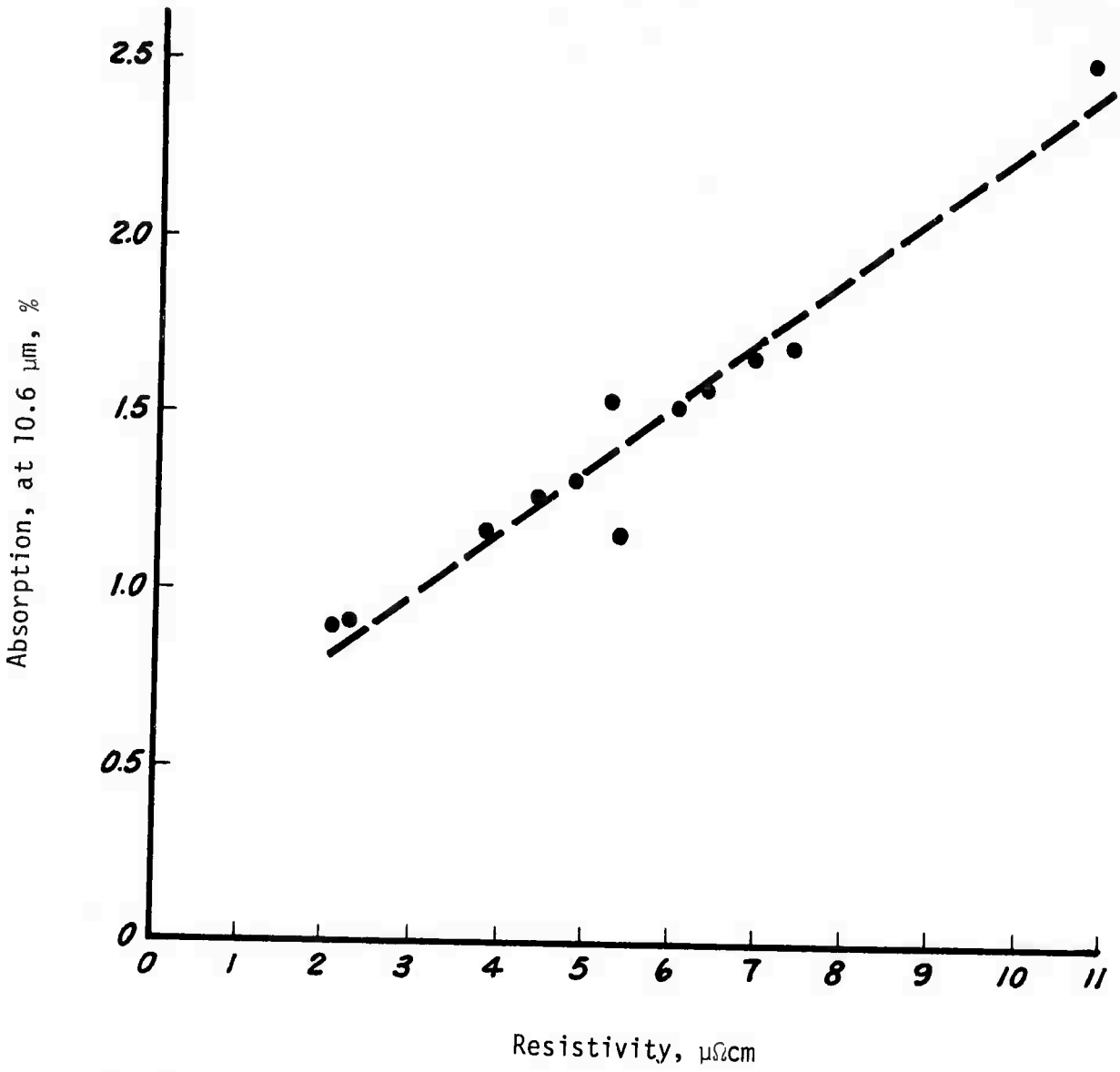

FIGURE 14. Measured Absorption at 10.6 µm versus Electrical Resistivity of the Sputtered Deposits--Absorption Values Were 5-10% Below Those Predicted by the Modified Drude Theory.(1)

(1) H.E. Bennett and J.M. Bennett, "Validity of the Drude Theory for Silver, Gold and Aluminum in the Infrared," Optical Properties and Electronic Structure of Metals and Alloys, North Holland, Amsterdam, p. 175, 1966.

CONCLUSIONS

The conclusions reached concerning desirable material characteristics, and the depotition parameters necessary to attain them, together with qualifying comments are presented here.

1) The material should have a very fine grain structure (<0.4 μm diameter).

2) This grain structure should be stable with respect to recrystallization for long time periods at expected handling and service temperatures.

3) With the dispersion hardening approach of meeting the characteristics of 1 and 2 above, the composition and deposition parameters should be such that a minimum microhardness value of 230 DPH be attained. It cannot be determined from the present results whether a higher hardness would be desirable.

4) No significant difference in polishability was observed between deposits hardened with alumina and those hardened with silicon carbide. However, the deposition behavior of the latter was more favorable, so silicon carbide will be used in continuing work.

5) Deposition parameter values favoring the development of a fine grain structure are:
   a. Composition: High % dispersoid
   b. Deposition rate: High
   c. Substrate temperature: Low

6) Deposition parameter values favoring the stability of a given grain structure are:
   a. Composition: High % dispersoid
   b. Deposition rate: Low to moderate
   c. Substrate temperature: High
   d. Substrate bias: Ground or floating

7) The thermal conductivity of the deposit will decrease with increasing vol% dispersoid. Since the energy-handling ability

of a mirror with a given reflectivity depends on its heat dissipation, it is desirable to use no more dispersoid than necessary. This consideration becomes more important if the dispersion hardened copper is to be used as a structural part of the mirror rather than as a thin coating.

8) The quality of the final polished surface depends to some degree on the quality of the as-deposited surface. Growth defects occur as a result of either particulate matter on the substrate or the effects of electrical arcs during the deposition. These defects contain and are surrounded by metal with a different character than the bulk of the deposit. The different character, which involves qualities such as porosity, weakly bonded interfaces, defect density, etc., manifests itself through accelerated polishing and/or etching rates. Such defects should be minimized to prepare the smoothest possible polished surfaces.

9) Given present sputtering equipment, a deposit with fewer growth defects can be made at a low deposition rate (e.g. 2 μm/min) rather than at a higher rate. The difference arises from the effect of voltage and current level on the frequency and intensity of arcing and from the ability to use transistorized current limiters in place of vacuum tube limiters when the target voltage is low (<500 V).

On the basis of the above considerations, the parameter values selected for further work are:

Composition: 1.0 vol% silicon carbide in copper
Deposition Rate: 2 μm/min
Substrate temperature: ≤50°C
Substrate bias: 0 or -20 volts
Substrate surface: Metallographic polish plus brief electropolish

RESEARCH IN SECOND PHASE OF PROGRAM

HIGH CONDUCTIVITY OVERLAYER

The principal goal of the second phase will be to determine if a thin sputtered copper overlayer (1000 - 2000 Å) will result in increasing reflectivity of the mirror to a minimum of 99.3%. Such results have been achieved[1] on low roughness surfaces (≤15 Å rms) by UHV evaporation of a copper overlayer. Depending on the results obtained from sputtered layers, UHV evaporated layers may be employed.

DISPERSION HARDENED DEPOSITS

Further evaluation of the deposits already made will continue to include neutron activation analysis for accurate determination of the deposit composition. Dispersion stabilized deposits will also be made and characterized on mirror supports of TZM, Mo and BeCu.

LASER DAMAGE

Experiments will be initiated to determine the extent and character of damage produced on mirrors with overlayers by their exposure to high energy laser pulses at λ = 10.6 μm.

REFLECTIVITY ENHANCEMENT COATINGS

Work will be inititated on $\lambda/4$ reflectivity enhancement coatings at a time dictated by the progress made on high conductivity overlayers. The selection of dielectric materials and an associated deposition technique will be made on the basis of a review of technology conducted during the second phase.

(1) H.E. Bennett, private communications.

ACKNOWLEDGMENTS

The author wishes to recognize the contributions of R. A. Bush, H. R. Gardner, R. L. Gordon, B. P. Hildebrand, N. Laegreid, L. L. Nichols, J. F. Williford and other staff members of the Battelle-Northwest Laboratories.

APPENDIX A

RELATIVE SCATTERING INSTRUMENT

APPENDIX A
RELATIVE SCATTERING INSTRUMENT

INTRODUCTION

A scattered light measuring instrument was built and tested. It is not an absolute measurement device, because it relies on a reference surface of known roughness. It consists of a sample holder in which two mirrors can be mounted and moved into the beam of light. A 1 MW He-Ne laser impinges on the mirror at 5° from normal. The light scattered into an 8° cone is gathered by a photomultiplier and measured. The center of the cone can be scanned through an arc 75° from normal. An additional measurement of the incident and specularly reflected light is made by using a beam splitter, a shutter arrangement and a phototransistor circuit. These measurements are made for a standard and a test mirror. The accepted formula for scattering from a rough surface with Gaussian statistics can then be used to find the rms roughness of the test mirror.(1)

SYSTEM DESCRIPTION

Figure A-1 is a system diagram for the measuring instrument. The lens and ground glass screens in the specular and incident measuring circuit are used to negate measurement variations due to a lack of perfect parallelism between the standard and the test mirror surfaces. A slight shift in the specular direction causes negligible change in light level at the phototransistor because (1) the lens focuses on almost the same spot on the first ground glass screen even though the direction of the incident ray changes and (2) the two ground glass screens scatter the light uniformly in spite of small changes of incident direction.

(1) H.E. Bennett and J.O. Porteus, "Relation Between Surface Roughness and Specular Reflectance at Normal Incidence." J. Opt. Soc. Am., vol. 51, pp. 123-129, 1961.

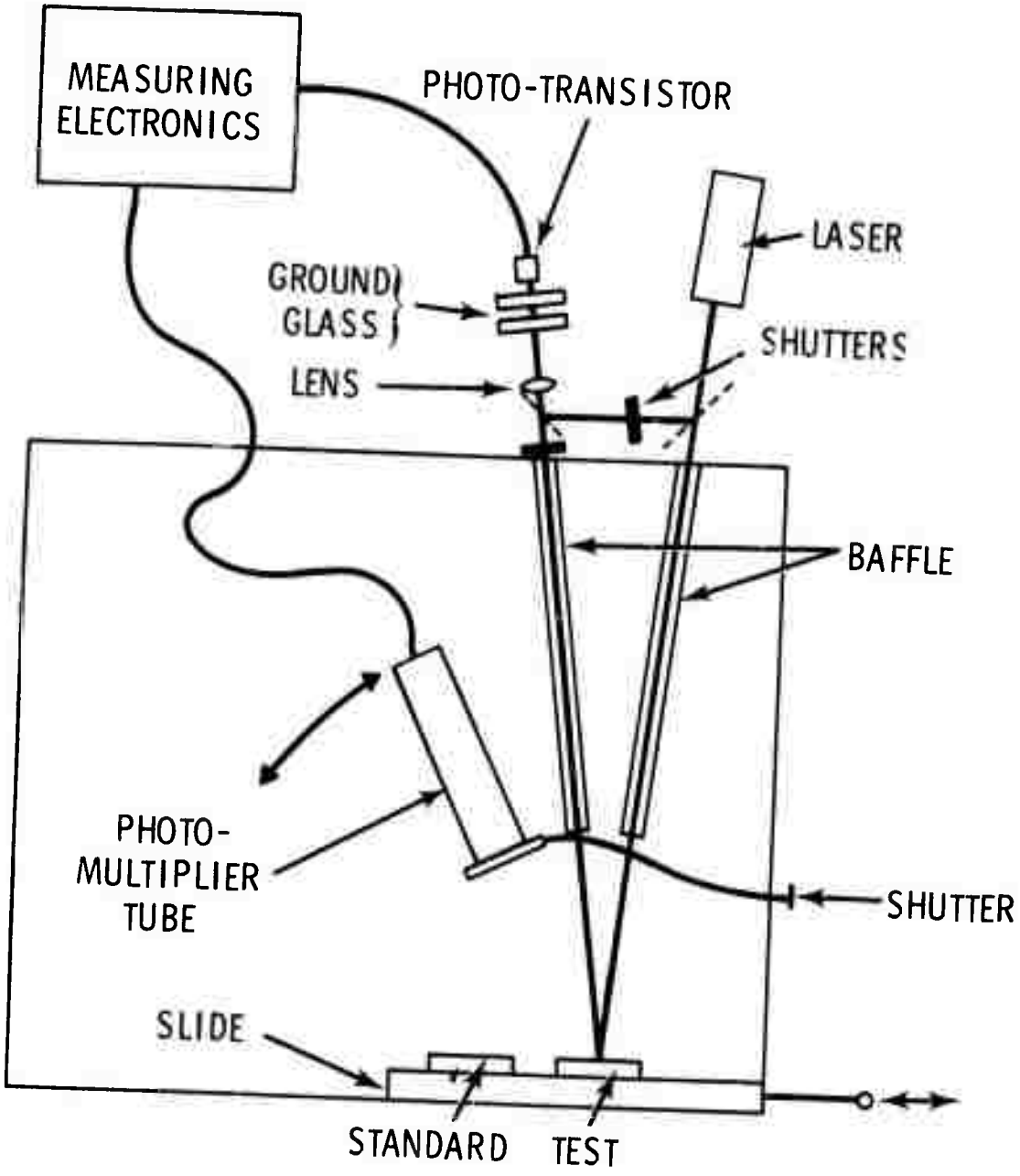

FIGURE A-1. Schematic Diagram of Relative Scattering Instrument

The incident and specular light measurement circuit itself is shown in Figure A-2. It consists of a MRD 3056 phototransistor connected to an LM-301-AN integrated circuit operational amplifier. The sensitivity of this detector is 0.4 so that a 1% change in intensity is easily measured.

The scattered light measurement circuit is shown in Figure A-3. An EMI 9658R photomultiplier tube with a Philbrick Nexus 140802 operational amplifier built into the tube socket provides ample sensitivity for these measurements. It was found that 800V was a sufficiently high voltage to operate the tube at high signal-to-noise ratio. So far, it has not been necessary to use a lock-in amplifier. The signals go to a strip chart recorder directly from the system.

Since the instrument does not measure absolute values, the ratio of scattered light/specular light is used. This necessitates a division operation. Since this can become tedious when many runs are made, an analog divider (Philbrick Q3-MIP multiplier-divider) is used to obtain the ratio of the two outputs. This ratio is then recorded on a strip chart recorder as a function of scattering angle. Data are reduced according to the analysis given in the text.

Reduced representative scattering data are shown in Figures A-4 to A-7. Experience with the instrument led to the following standard procedure. Each sample was first provided with reference marks separated by 90° in the plane of the sample. A horizontal scan was obtained along the arbitrarily chosen axis with the PM tube fixed at $\theta = 25°$ by manually sliding the sample under the incident beam a distance equilent to the sample width. Thus, a position producing minimum scattering was chosen. The PM tube was then moved through $20° < \theta < 75°$ and the data recorded. The sample was then rotated 90° and the procedure repeated. Sample data, thus, produced are compared to those obtained from the position of minimum 25° scattering from the standard. Positions at which data were taken are indicated on the figures.

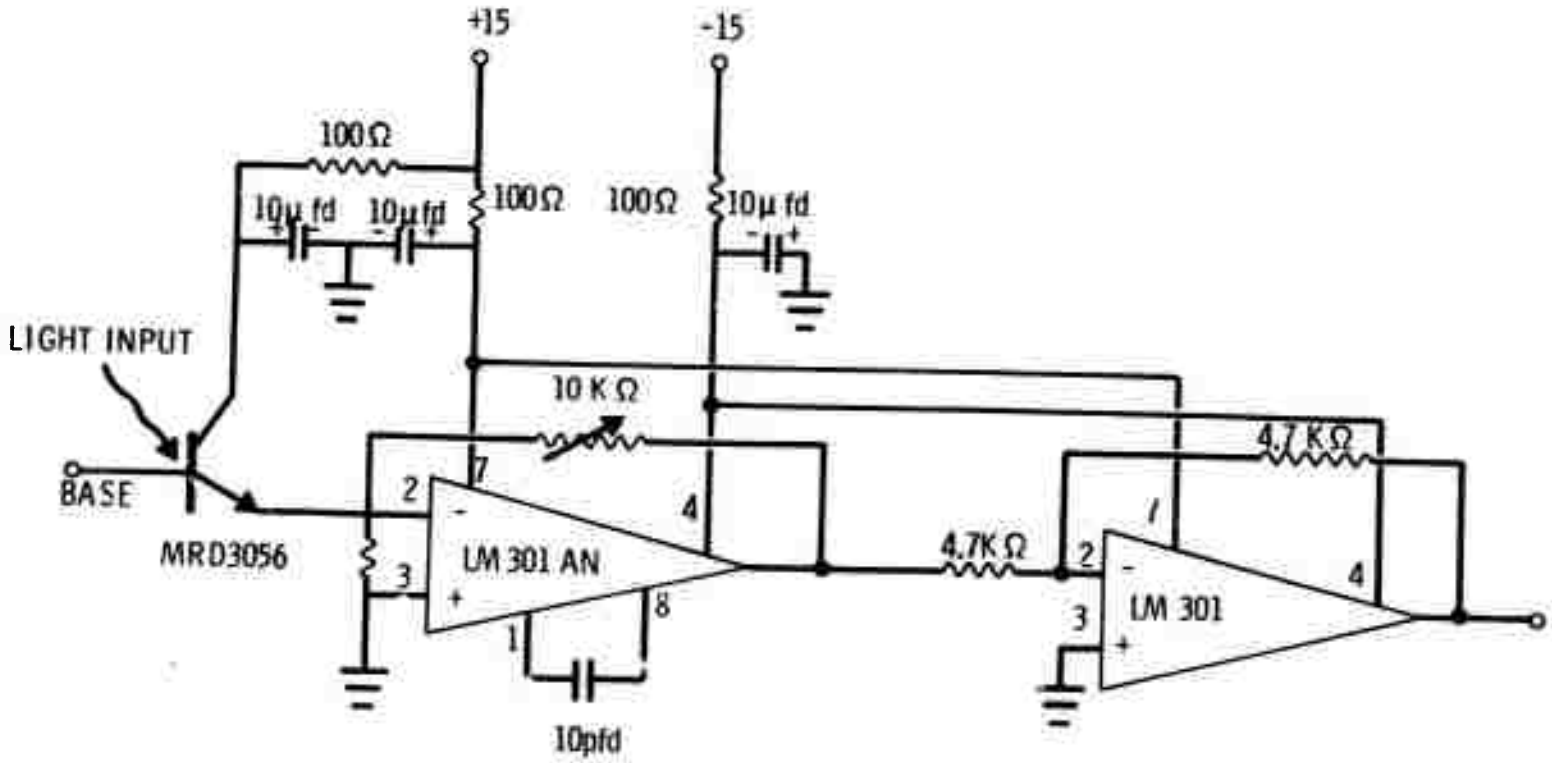

FIGURE A-2. Measurement Circuit for Incident and Specularly Reflected Light

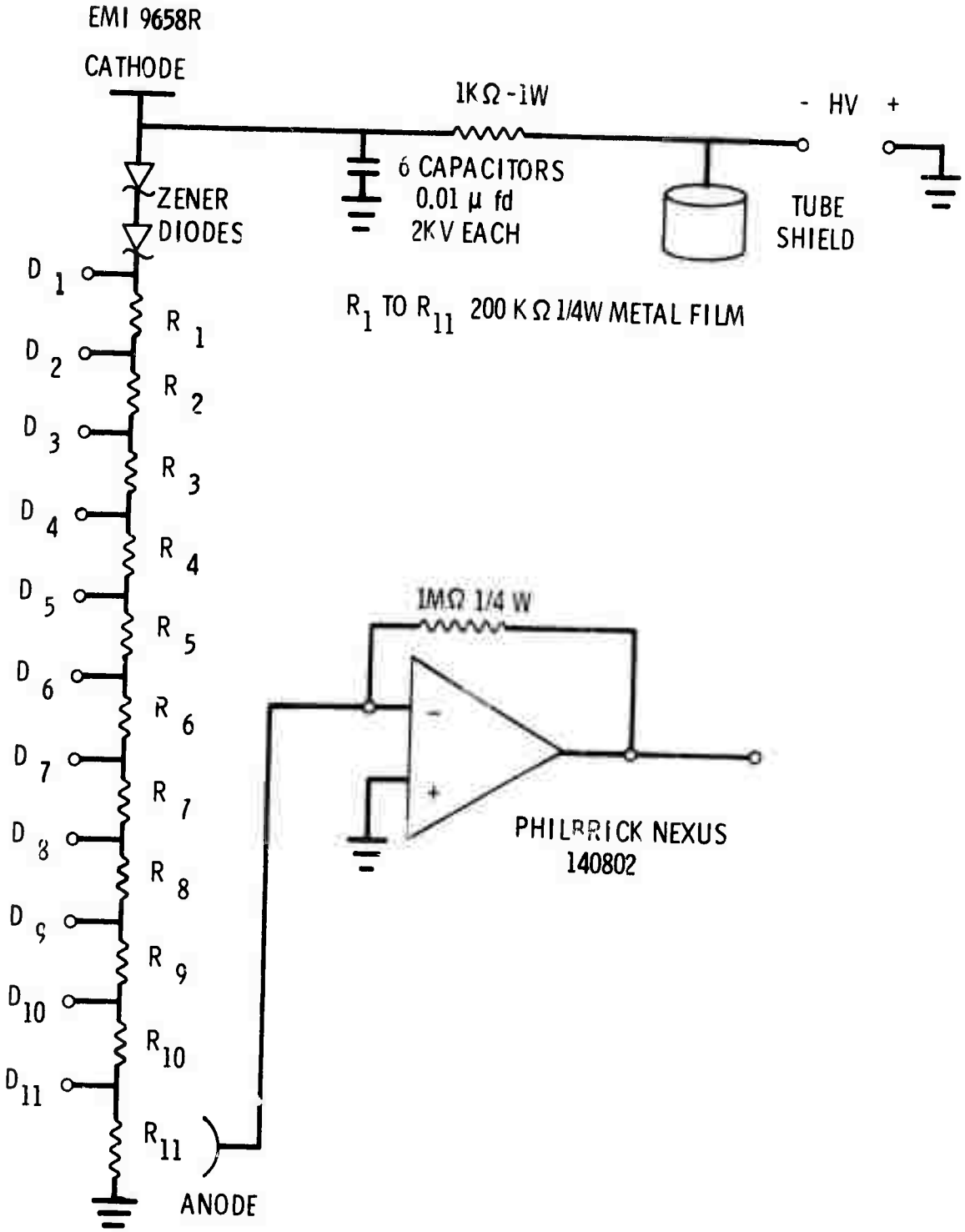

FIGURE A-3. Scattered Light Measurement Circuit

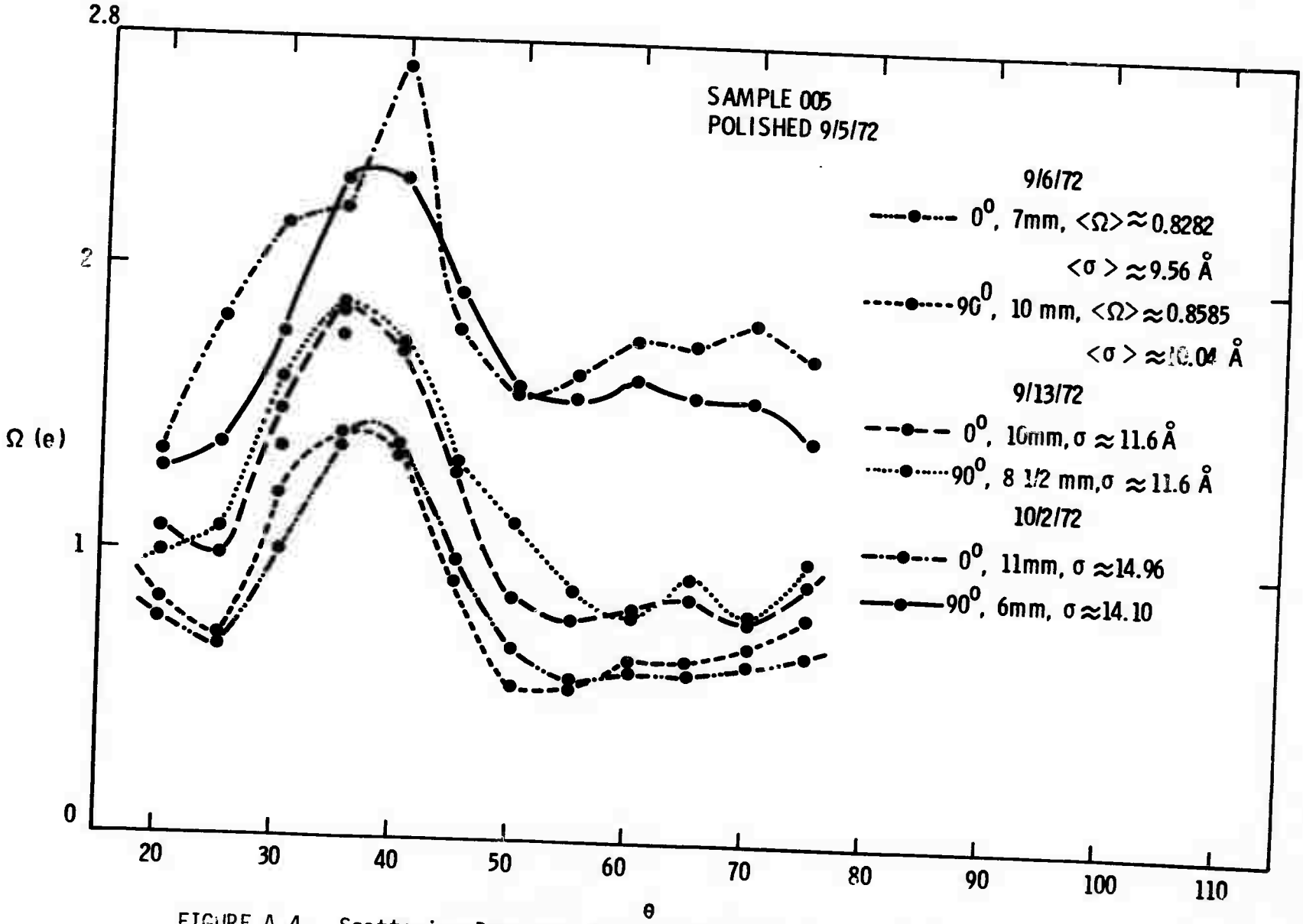

FIGURE A-4. Scattering Data for Sample 005 (1% SiC, 50V Bias, Cold)-- Positions at Which Data Were Obtained Are Shown on the Graph. Note the General Increase in Roughness with Time.

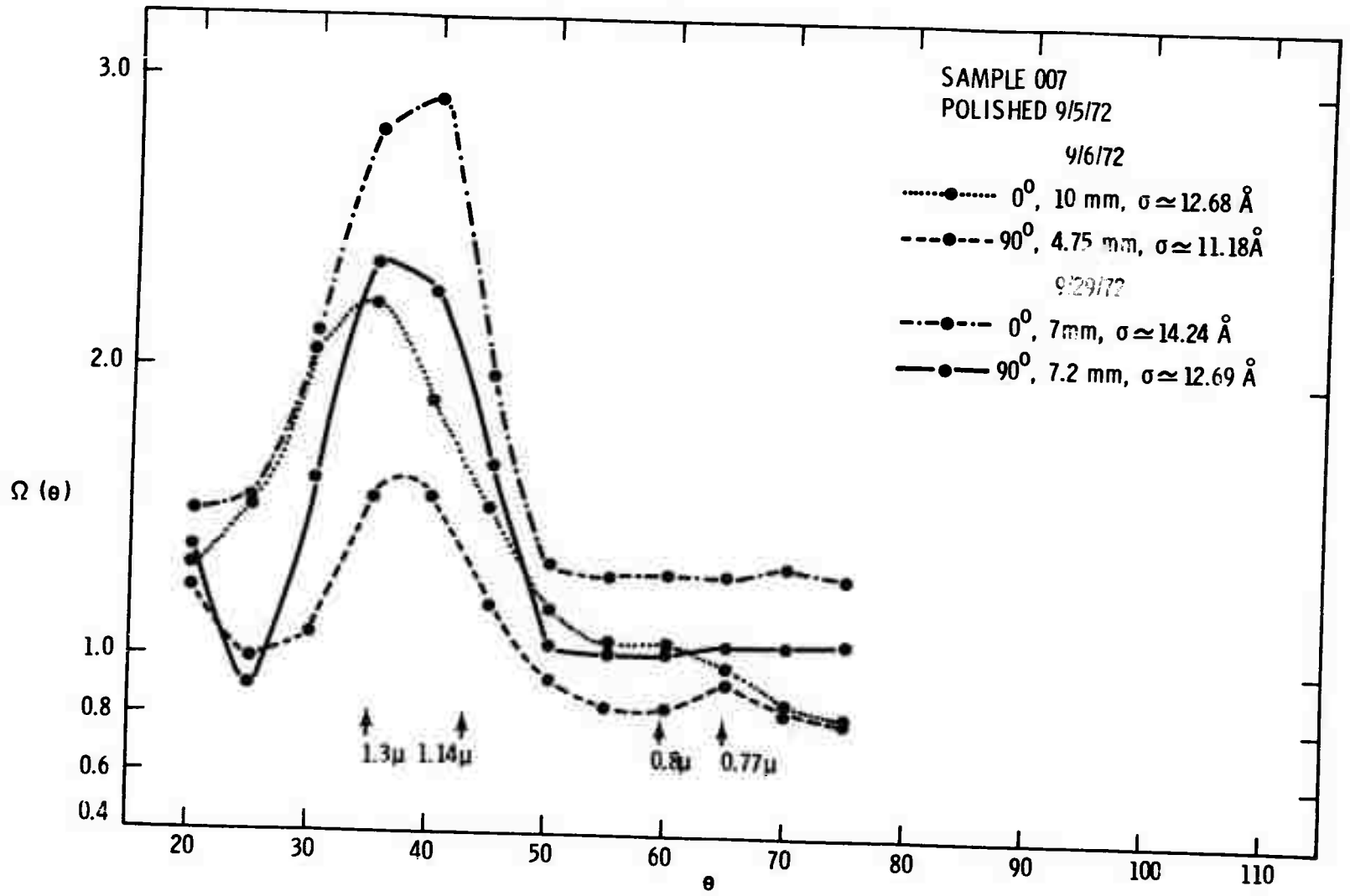

FIGURE A-5. Scattering Data for Sample 007 (0.25% SiC, Floating, Cold)--- Spatial Wavelengths of Surface Structure Corresponding to Scattering Maxima are Indicated by Vertical Arrows.

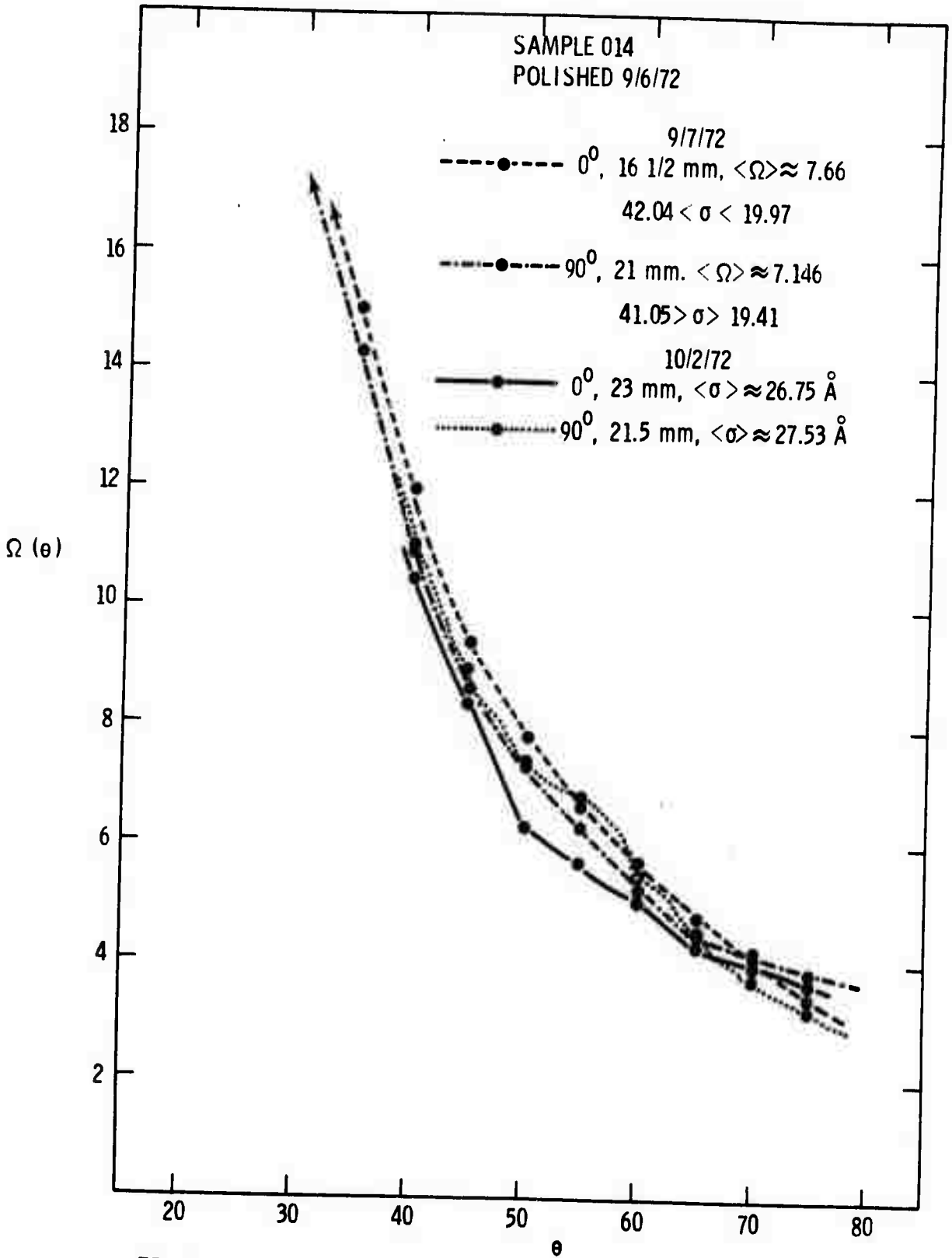

FIGURE A-6 Scattering Data for Sample 014 (1% SiC, Floating, Cold) Deposited on an As-Machined Support.

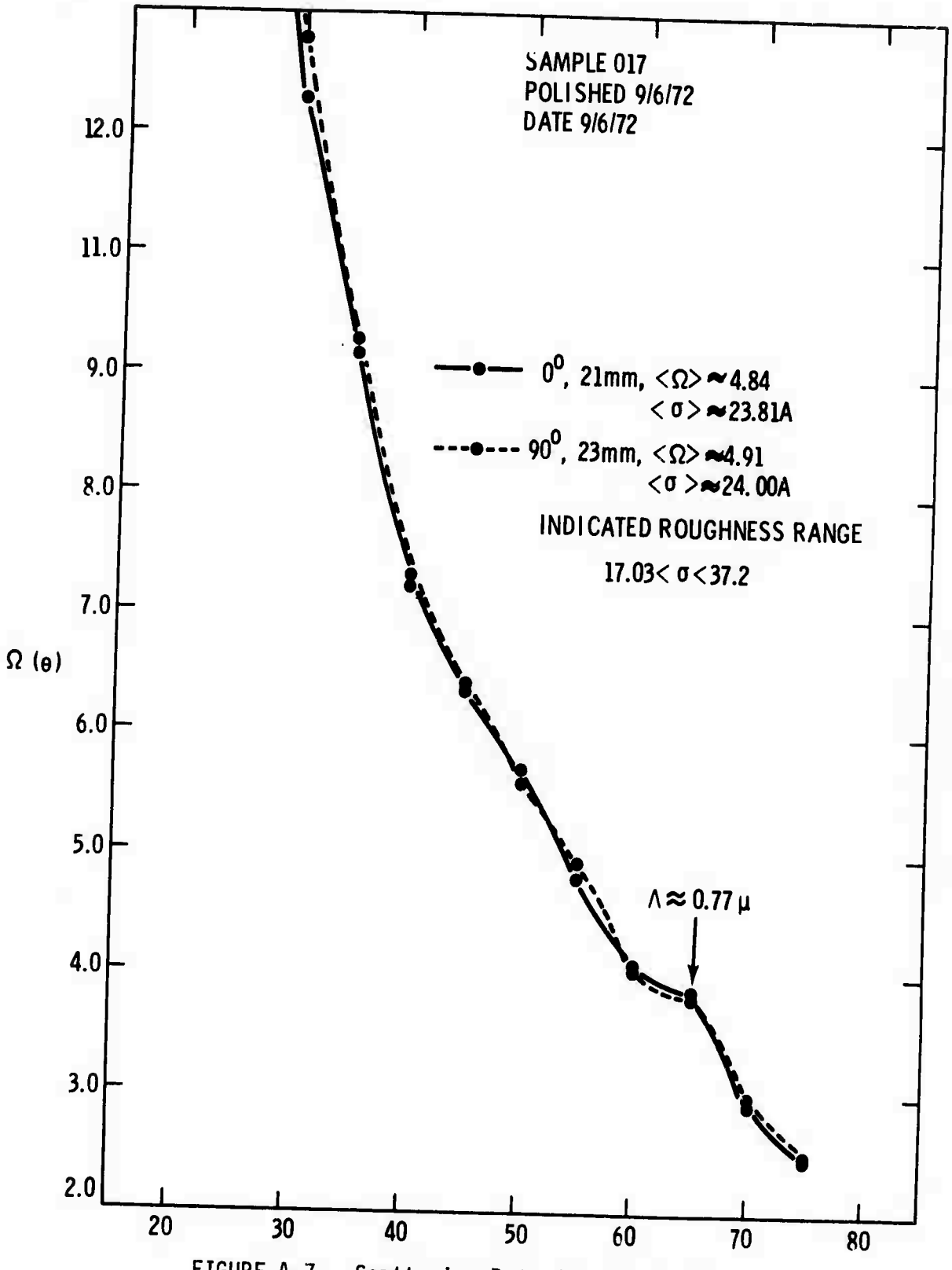

FIGURE A-7. Scattering Data for Sample 017 (2% SiC, Floating, Cold Water)

Figure A-4 shows scattering data obtained on Sample 005 (1% SiC, 50V bias) over the period from September 6, 1972 through October 2, 1972. During the interval the sample was stored in a nonvacuum dessicator jar. The surface roughness of this sample increased from 10 Å rms to about 15 Å rms during this time period. This behavior was found to be typical of the smoothest surfaces produced, as evidenced by the results shown in Figure A-5 for Sample 007 (0.25% SiC, floating). The surface changes could be detected on Nomarski DIC photographs, but the identity of the surface contaminant and the detailed mechanism of degradation is not known at this time. In some cases the initial surface roughness could be restored by washing in Ivory detergent and cold water. More experience must be gained to determine the nature and the cause of both reversible and irreversible surface degradation.

Figure A-5 also shows the range in spatial wavelengths of surface periodicity indicated by the observed angular distribution of scattered light. The wavelengths are derived from Equation 5 in the text.

Figures A-6 and A-7 are typical of scattering results obtained from some samples exhibiting a rougher surface. Although numbers for surface roughness are indicated on these graphs, the actual rms roughness is probably greater than that shown. The approximations used in the analysis are suspect in situations typified by Samples 014 and 017. Until corroborating data on rough samples are received the instrument will be used only as an independent indicator, providing verification of Nomarski DIC results.

APPENDIX B

THEORETICAL ANALYSIS, PRELIMINARY DESIGN AND ESTIMATED COST FOR A LABORATORY DEMONSTRATION OF AN OPTICAL HETERODYNE SURFACE PROFILE INSTRUMENT

APPENDIX B
THEORETICAL ANALYSIS, PRELIMINARY DESIGN AND ESTIMATED COST FOR A LABORATORY DEMONSTRATION OF AN OPTICAL HETERODYNE SURFACE PROFILE INSTRUMENT

INTRODUCTION

The general principle of the optical heterodyne interferometer used for the measurement of surface vibrations is well described by Massey.[1] Vibrations with amplitudes of 0.02Å have been measured with this technique; the theoretical capability is at least one order of magnitude better (0.002Å).[2] The adaptation of this technique to surface profile measurement in the same range of amplitudes is described in a paper presented to the Interagency Mechanical Operations Group (IMOG), Subgroup on Gaging Meeting No. 33, June 1972.[3]

GENERAL PRINCIPLE OF OPERATION

The basic interferometer is sketched in Figure B-1. A laser beam is passed through an acoustic Bragg cell driven at 25 MHz. The result is two light beams, one at the original optical frequency and the other up-shifted by the 25 MHz driving frequency. The up-shifted beam is diffracted through the angle $\alpha = \sin^{-1}\lambda/2\Lambda$ where λ is the optical wavelength and Λ is the acoustical wavelength. This angle allows the two beams to be easily separated by the wedge beam splitter or prism. One beam is focused onto the sample. The reflected light is gathered

1. G.A. Massey, "A Laser Instrument for Vibration Measurement," Optical Spectra, January/February 1969.
2. R.L. Whitman, L.J. Laub and W.J. Bates, "Acoustic Surface Displacement Measurements on a Wedge-Shaped Transducer Using an Optical Probe Technique," IEEE Transactions SU-15, vol. 186, 1968.
3. B.P. Hildebrand, "Surface Roughness Measurement by an Optical Heterodyne Technique," Minutes of IMOG Subgroup on Gaging, 33rd Meeting, 1972.

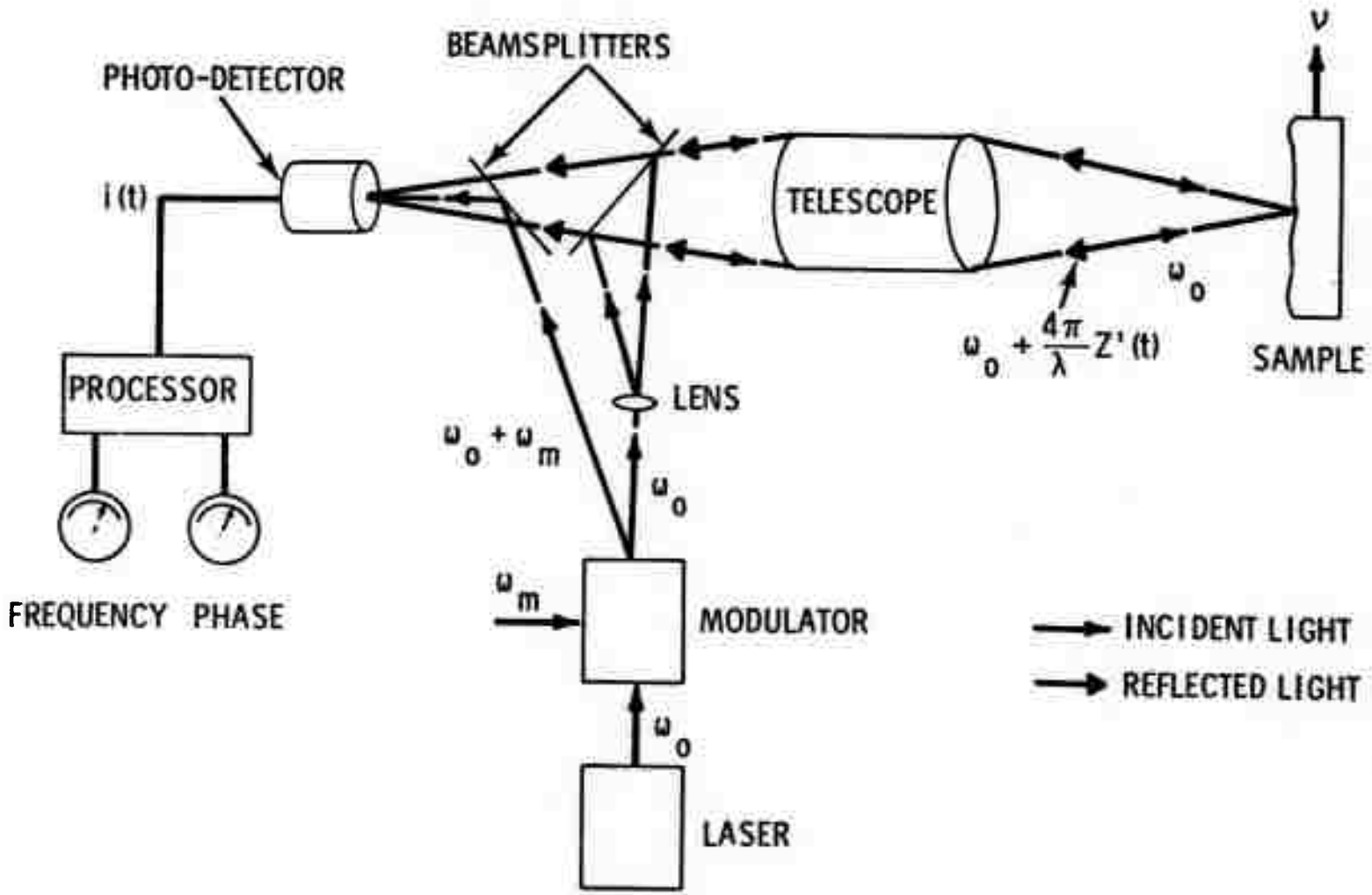

FIGURE B-1. Heterodyne System for Surface Profile Measurement

by the same optical system used to focus the beam and diverted to a photodetector. The other beam is directed to the photodetector directly. The square-law behavior of the photodetector results in an electronic signal centered around the microwave frequency. A vibration of the sample will impose a doppler shift on the sample beam resulting in a shift of the frequency of the signal; this can be related to the amplitude of vibration.

Surface profile measurement using this technique induces the same type of effect on the sample beam by translation of the sample past the beam. If, for example, the surface were corrugated with a spatial period a, then a translation velocity of v would result in a signal frequency shift of v/a, the amplitude of which is proportional to the depth of the corrugation. Thus, such a device would need to be followed by an electronic frequency tracker to provide the necessary measurement. For rough measurements, the signal could be fed to a spectrum analyzer; the display would graphically show the amplitude distribution of the surface corrugations as a function of spatial frequency.

OPTICAL SYSTEM

The optical system must be designed so that the two beams impinging on the photodetector are matched in curvature and direction. If this is not done, different regions on the photodetector will observe the signal with different phase shifts, with the result that the current output will be attenuated. In order to compensate for irregularities or vibration of the translation stage, the reference beam should also be directed onto the sample or a reference mirror mounted on the stage. This beam should be defocused so that it is not affected by the roughness but only by the vibration.

Ideally, the reference beam should cover the same region on the sample on which the sample beam is focused. However, the optics involved become quite complicated; hence, the separate beam approach

described above will be tried. Hopefully the translation stage will vibrate as a unit with no relative rotational motion. A sketch of the proposed optical system is shown in Figure B-2. The optics are arranged so that both return beams are collimated. The microscope objectives are identical (within manufacturing tolerance) so that the return beams will be matched.

RESOLUTION

The spot size of the focused beam is expressed as

$$d = 2.44\lambda F$$

where F is the f-number of the lens and d is the diameter to the first dark ring of the diffraction spot. This formula assumes a uniform field across the entrance pupil. The transfer function of such a system is low-pass with sharp cutoff at the spatial frequency of $f_o = 1/2\lambda F$. Thus, for an F-1 objective and $\lambda = 6328\text{Å}$, spatial periods of $1/f_o = 2\lambda F = 1.26$ μm can be resolved. Corrugations with smaller period will not be seen.

Since a laser beam does not have a uniform spatial amplitude distribution, the resolution is not as shown above. The spot size for a Gaussian profile entrance beam can be written as

$$d \simeq \frac{4}{\pi} \lambda F$$

where d is now the diameter at which the spot intensity falls to $1/e^2$ of maximum. Since, the Fourier transform of a Gaussian function is also Gaussian, no sharp cutoff in spatial frequency occurs. However, the effective bandwidth will not be much different than before, but the higher spatial frequencies will be attenuated. This will have to be taken into account in the signal processing; that is, gain compensation will need to be performed at the higher frequencies. This can easily be done by electronic filtering.

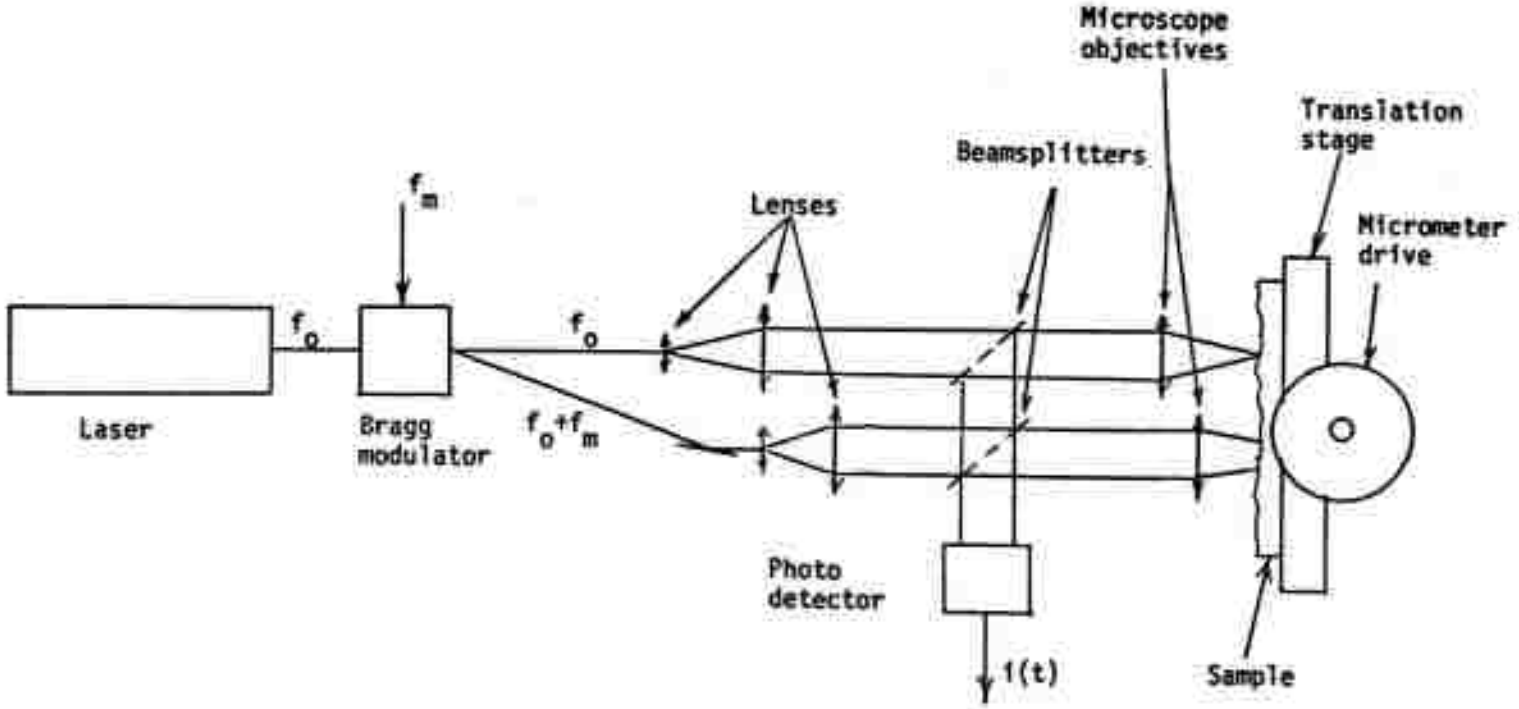

FIGURE B-2. Optical System for Surface Profile Measurement

DEPTH OF FOCUS

The depth of focus for the spot is also of interest. An expression for depth of focus is

$$D = 2\lambda F^2$$

where D is the distance along the optical axis for which the intensity remains within 80% of maximum. For our example, D = 1.26 μm. This does not become a problem, because the research only necessitates working with surface variations of less than $\lambda/2 \cong 0.3$ μm.

EFFECT OF SURFACE SLOPE

A corrugated surface presents certain problems different from those presented to a vibration measurement application; namely, as the sample is translated past the beam, the surface normal changes direction. Thus, the reflected light changes in direction with a possible loss of collected light. A simple calculation can be performed to ascertain this effect.

The maximum slope presented to the light beam is $s = 2\pi f_o a$ with the amplitude of the surface corrugation.

Since $s = \tan\theta$, with θ the angle the surface makes with the horizontal plane, the angle the surface normal makes with the optical axis is

$$\theta = \tan^{-1}(\pi a/\lambda F).$$

For our example this becomes

$$\theta = \tan^{-1}(5 \times 10^{-4} a).$$

The acceptance angle of the microscope objective can be written as

$$\psi = \tan^{-1} 1/F$$

$$= 45° \text{ for } F = 1.$$

If the angle θ is small with respect to acceptance angle ψ, no significant problem with slope variation will be expected. This idea can be written as the inequality

$$\theta \simeq \frac{\pi a}{\lambda F} << 1$$

$$\text{or } a << \frac{\lambda F}{\pi} \sim \frac{\lambda}{3}.$$

We have assumed $\tan \theta \simeq \theta$.

Since the aim of the research is to measure surfaces with roughness in the neighborhood of $10^{-2}\lambda$ or less, the surface slope will not affect the measurements to any appreciable extent. If the instrument is to be used on much rougher surfaces, special collecting optics will need to be designed.

DISCUSSION

The optical system required is quite simple, consisting of a Bragg cell, two microscope objectives and a number of beam splitters. An additional component may be needed--a directional coupler to prevent the reflected beams from returning to the laser. This can be done with a quarter wave plate and calcite prism and should offer no problem. It will be done only if laser fluctuations due to interference with the reflected beams are observed.

An F-1 lens offered the capability of resolving spatial variations of 1.26 μm. If greater resolution is required, it may require the use of oil immersion lens systems. In this case the f-number may decrease to as little as F-0.36, giving a resolving capability of 0.45 μm. Particularly with the immersion lenses, the use of these low f-number

lenses presents practical problems such as short working distance. The typical F-1 lens, for example, has a working distance of about 1.6 mm, whereas the typical F-0.36 lens will have a working distance of only 0.1 mm. This is large on the scale of roughness but small on the scale of mechanical construction of the sample stage and lens mounting.

ELECTRONICS

The input to the electronic measurement system is

$$i(t) = C_1 + C_2 \cos \left[2\pi f_m t + \psi(t)\right]$$

where

f_m = rf modulation frequency

$$\psi(t) = \frac{4\pi}{\lambda} Z(t)$$

$Z(t)$ = deviation of the surface from a datum plane.

Let $Z(t)$ be one Fourier component of the roughness, namely a $\sin 2\pi f_1 t$. Then

$$i(t) = C_1 + C_2 \cos \left[2\pi f_m t + \frac{4\pi a}{\lambda} \sin 2\pi f_1 t\right] .$$

This can be expanded in a Bessel function series

$$i(t) = C_1 + C_2 \left[J_o\left(\frac{4\pi a}{\lambda}\right)\cos 2\pi f_m t + \sum_{n=1}^{\infty} J_n \left(\frac{4\pi a}{\lambda}\right)\cos 2\pi (f_m + nf_1)t\right]$$

$$- \sum_{n=1}^{\infty} J_n \left(\frac{4\pi a}{\lambda}\right)\cos 2\pi \left(f_m - nf_1\, t\right) .$$

For small argument

$$J_o(x) \simeq 1$$

$$J_1(x) \simeq x/2$$

$$J_n(x) \simeq 0 \text{ for } n > 1 \quad .$$

Hence

$$i(t) \simeq C_1 + C_2 \left\{ \cos 2\pi f_m t + \frac{2\pi a}{\lambda} \left[\cos 2\pi \left(f_m + f_1 \right) t - \cos 2\pi \left(f_m - f_1 \right) t \right] \right\} .$$

This represents a signal centered on f_m with two sidebands at $f_m \pm f_1$; the amplitude is a direct measure of the roughness amplitude. Thus, the electronics simply serve to isolate one of the sidebands, track its frequency and measure its amplitude. The frequency spread and consequently, the bandwidth of the system is determined by the spatial bandwidth of the optical system, the spatial spectrum of the surface and the velocity of translation. Assuming the spatial spectrum of the surface to be greater than the optical bandwidth, the resulting frequency bandwidth is

$$B = vf_o = \frac{v}{2\lambda F}$$

where

v = velocity of scan.

A scan velocity of 1 mm/sec, for our example, yields a bandwidth of 800 Hz. The bandwidth, in turn, limits the sensitivity of the amplitude measurement since it determines the noise allowed into the system. If it is assumed that a signal-to-noise ratio of one is acceptable, the following equations can be used to obtain

$$Z_{min} = \left(\frac{hc\lambda B}{\pi^2 \eta P_o} \right)^{1/2}$$

where

h = Planck's constant
c = velocity of light
η = quantum efficiency of the detector
P_o = laser power .

For typical values, $\eta = 5 \times 10^{-2}$, $P_o = 1$ MW we obtain

$$Z_{min} = 3.8 \times 10^{-3} \text{ Å} \quad .$$

Higher laser powers are easily available, 500 MW from an argon ion laser is common. This would increase the sensitivity by more than an order of magnitude.

A block diagram of the electronic system is shown in Figure B-3. If a random surface is considered, the electronics is required to track the frequency

$$f = f_m + \frac{2}{\lambda} \frac{dz(t)}{dt}$$

which, for our example, can vary over an 800 Hz range. The voltage controlled oscillator (VCO) with negative feedback, shown in Figure B-3, serves this purpose. The output of the VCO is mixed with the amplified and filtered signal to yield a beat at the difference frequency. This signal is integrated by a low-pass filter, yielding an error signal applied to the frequency tuning terminals of the VCO as negative feedback. This forces the VCO to track the incoming signal. The error signal then represents the desired demodulation of the input. This provides a direct indication of the normal velocity of the surface. To obtain displacement, the error signal will have to be integrated over the bandwidth expected (800 Hz for our example). The limiter in the control loop serves to make the demodulation independent of variations in amplitude due to equipment vagaries.

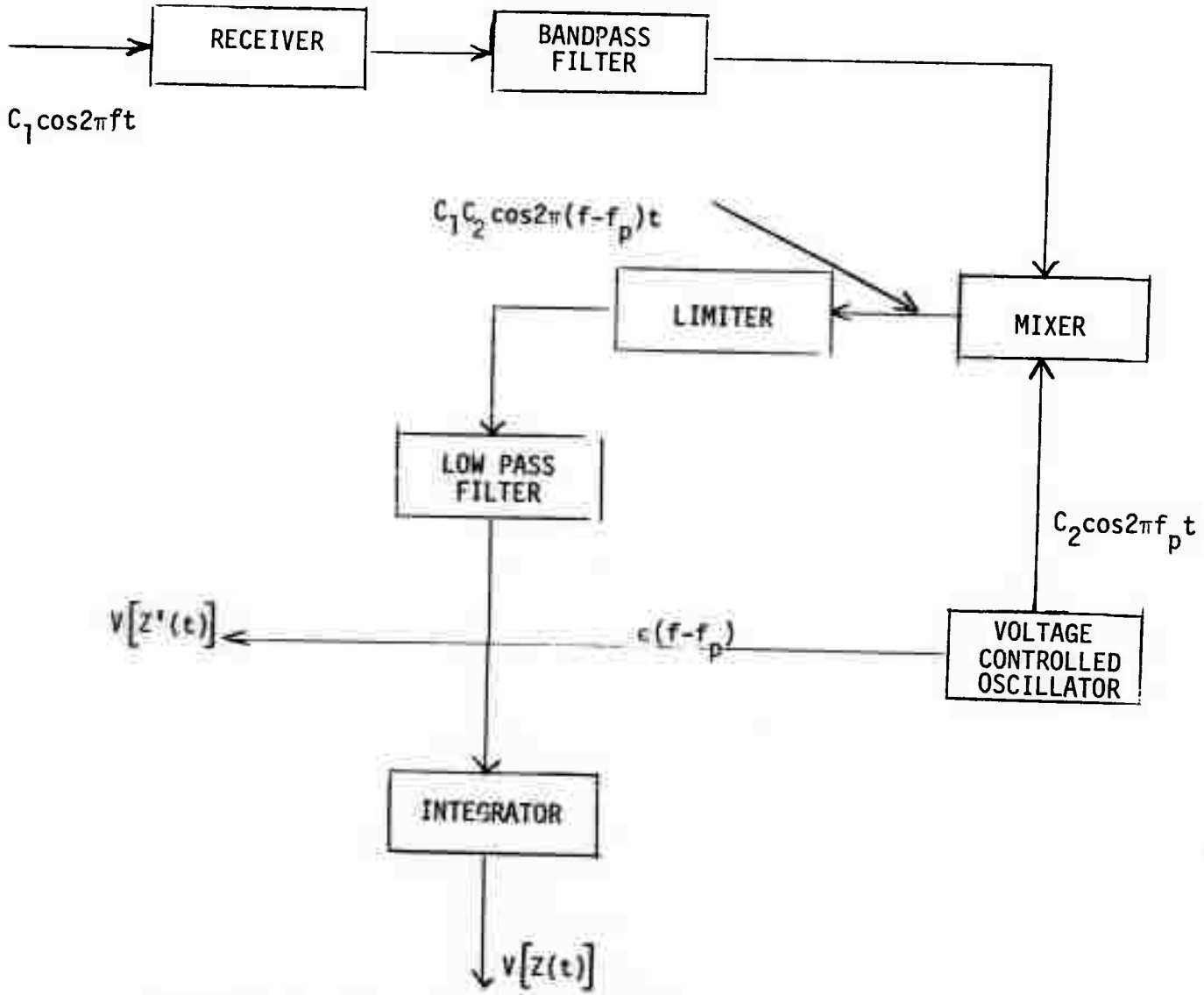

FIGURE B-3. Diagram of Electronic Measurement System

The electronic package needed to extract the roughness information from the signal is basically simple, requiring no sophisticated techniques; therefore, it should be relatively easy to build and since the information resides in a frequency shift, the measurement is absolute.

TIME AND COST ESTIMATE FOR EXPERIMENTAL DEMONSTRATION

This estimate is based on the availability of a laser and major cost electronic items such as RF receiver and chart recorder. The major cost in purchased components is the Bragg cell and driver. The major fabrication cost is the motor driven precision translation stage.

The time estimate is two months with one man-month scientist and two man-months of technician time. The total estimated cost is $25,000.

APPENDIX C

DIFFERENTIAL CALORIMETER

APPENDIX C
DIFFERENTIAL CALORIMETER

DESCRIPTION

A twin-type calorimeter design was chosen so that slow fluctuations in room temperature would be canceled out because each cell of the calorimeter would be affected identically. Also, an electrically heated mirror had to be mounted for calibration purposes followed by mounting an experimental mirror without changing the calibration constant. A permanently mounted reference mirror on one side of the twin calorimeter satisfied this criterion.

An exploded top view of the calorimeter is shown in Figure C-1. The reference mirror is thermally coupled to a 3.8 cm diameter by 0.38 cm thick aluminum disc using a commercial heat sink compound. The aluminum disc was glued to a 3.8 cm diameter by 1 cm thick piece of acrylic which was in turn glued to the temperature controlled jacket of the calorimeter system. A glass bead thermistor (resistance 3000 ohms at 25°C and dissipation constant 8 MW/°C) was thermally coupled into a small hole in the aluminum disc and its electrical leads were brought out through a 0.13 cm hole in the acrylic disc. The other cell of the calorimeter was constructed and assembled in an identical manner. The constant temperature jacket was machined from a 2.67 × 6.35 × 13.65 cm aluminum block. The perimeter of this block was wrapped with manganin wire to be used as an electrical heating coil. A thermistor was positioned in the aluminum jacket to monitor the jacket temperature. The unequal heat flow through each cell of the calorimeter made it necessary to put the calorimeter in a box to protect it from room air currents which caused short-term fluctuations in the calorimeter output. This acrylic box had a shutter which was opened only during the laser illumination period.

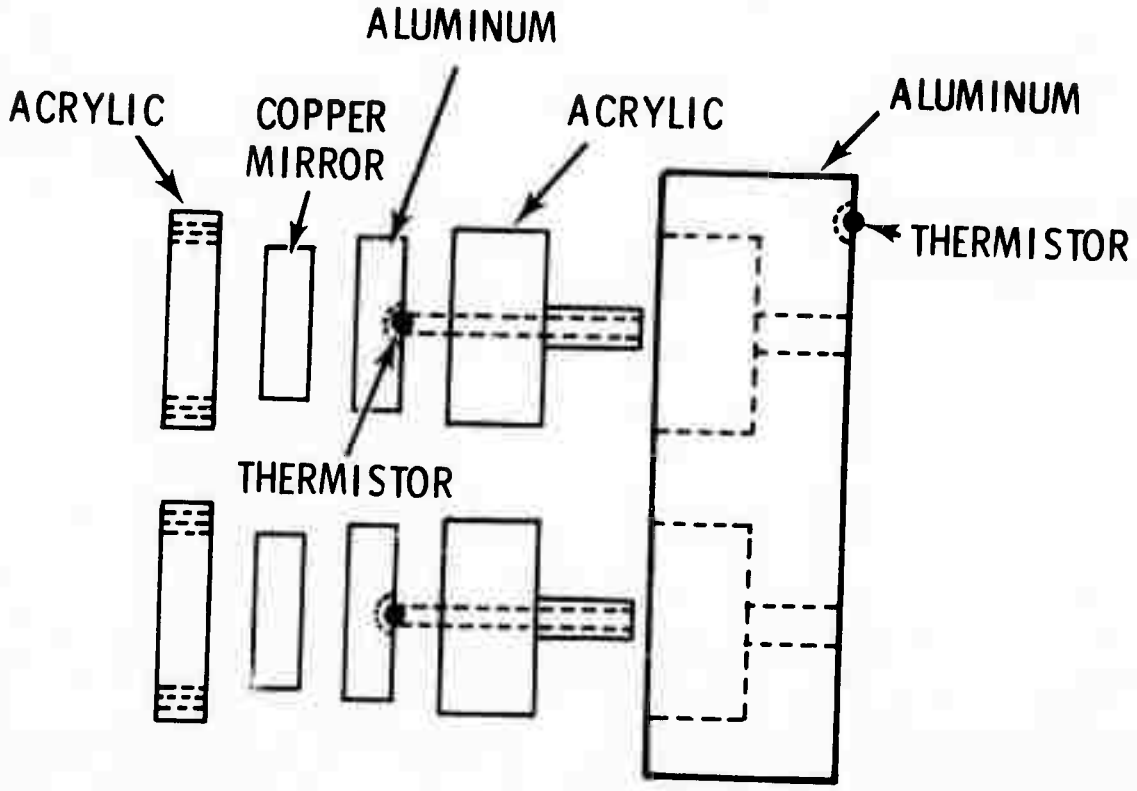

FIGURE C-1. Exploded Top View of Differential Calorimeter

The main electronic components consisted of a microvoltmeter, a 2-channel chart recorder, a power supply and two simple Wheatstone bridge circuits. Figure C-2 shows details of the electronic circuits.

The output of the jacket temperature bridge circuit was recorded on Channel B of the strip chart recorder. The Channel B retransmitting potentiometer was used to control an electronic switch which turned power on and off to the jacket heater coil. The temperature sensitivity of this bridge circuit is 0.0135 V/°C; the jacket temperature control is better than ±0.0018°C. This temperature control system is more than adequate for this calorimeter. The typical jacket operating temperature was 25°C with a room temperature of 22 to 23°C.

The thermistors in each cell of the calorimeter are on opposite arms of a Wheatstone bridge, and all elements have equal resistances at balance. The calculated temperature sensitivity of this circuit is 1.8×10^{-3} volts/°C when using a thermistor having a temperature coefficient of about 4%/°C. The nonlinearity of the thermistor introduces negligible error for the small temperature changes of ≈0.03°C used in the experiment. The output of this bridge circuit is amplified with a microvoltmeter and recorded on Channel A of the strip chart recorder. The cooling time constant of the calorimeter is 10 minutes.

CALIBRATION

The method of calibration for the calorimeter was to compare the power absorbed in a mirror directly to an electrical power of the same magnitude. This assumes that the systematic errors arising from temperature gradients are negligible or equal in both the calibration run and the mirror absorption run and, therefore, cancel each other.

A 1/8 Watt, 1000 ohm carbon resistor was imbedded in one of the mirror samples to be used for electrical calibration. This was accomplished by drilling a suitable hole through the diameter of one of the mirror samples near to the front surface. The carbon resistor was

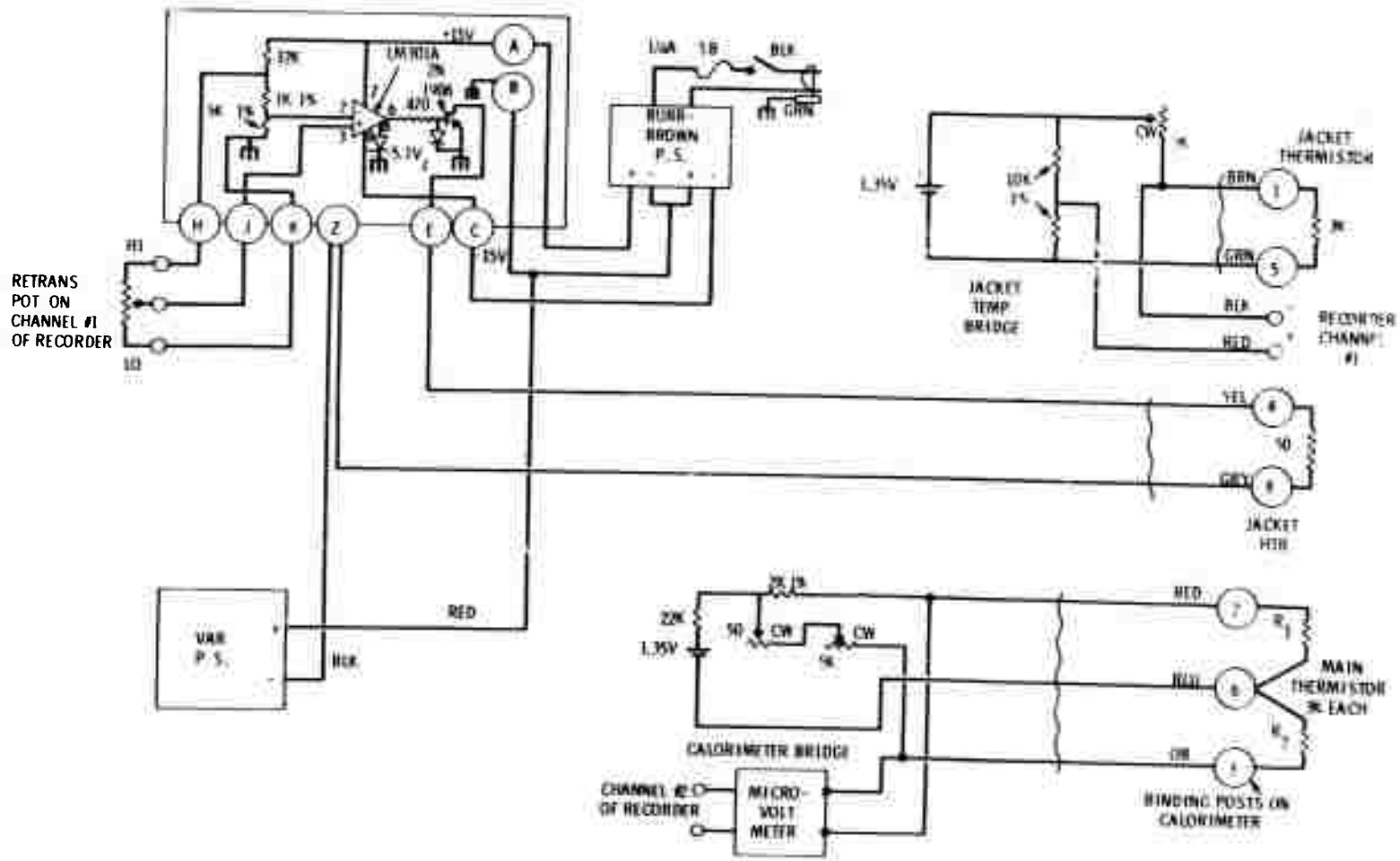

FIGURE C-2. Electronic Circuits for Differential Calorimeter System

centered in this hole and the remaining void space was filled with a commercial heat sink compound. The other components of the electrical calibration circuit consisted of a precision resistor in series with the carbon resistor, a digital voltmeter and a low voltage power supply. The precision resistor and voltmeter were calibrated against standards traceable to the National Bureau of Standards (NBS) at our Standards Calibration Laboratory. A calibration run consists of applying a voltage for 30 seconds (measured with an electrically timed switch) and of measuring the voltage drop across both the carbon resistor and precision resistor. From these data, an accurate determination of the electrical power input can be made. The integrated area of the time-versus-temperature graph from the calorimeter is compared to the electrical input to determine the calibration constant for the calorimeter in terms of joules per unit area on this graph.

The electrical calibration runs were performed several times during the time span covered by the experiment and the data were taken by more than one individual. Table C-1 shows the variation in the calibration constant during the time span covered. Calibration runs on the same date mean the runs were repeated without disturbing the mounting of the mirror, whereas data on different dates mean the mirror had been removed from the calorimeter and subsequently remounted using a new film of heat sink compound. The reference mirror mounted on the second cell of the calorimeter was not removed at any time during the duration of the experiment. The average value of the calibration constant derived from data in Table C-1 is A - 0.4799 ± 0.01 joule/in.^{2}, indicating a reproducibility of at least 2.1%. The overall precision of the calibration indicates an absolute accuracy of ±5% at the 95% confidence level. The absolute accuracy of the measurement of the absorption of an unknown mirror sample is estimated to be ±6% at the 67% confidence level.

TABLE C-1. Calibration Data for Differential Calorimeter

Date	Area of Time-Temperature Curve ($in.^2$)	Electrical Energy Input (joules)	Constant Calibration (joules/$in.^2$)
9-28-72	6.060	2.974	0.4907
9-28-72	6.318	3.007	0.4759
10-10-72	6.271	2.955	0.4712
10-10-72	5.964	2.958	0.4960
10-10-72	6.270	2.982	0.4756
10-24-72	5.994	2.865	0.4781
10-24-72	4.498	2.124	0.4722
10-24-72	7.124	3.455	0.4850
10-24-72	6.002	2.820	0.4698
10-24-72	5.722	2.820	0.4927
10-24-72	5.976	2.820	0.4718